Proceedings of the
Annual Stability Conference
Structural Stability Research Council
Pittsburgh, Pennsylvania, May 10-14, 2011

DSM design of cold-formed steel columns against distortional failure: numerical investigation on the influence of the cross-section geometry and support conditions

A. Landesmann[1], D. Camotim[2]

Abstract

This work reports the results of a numerical investigation on the influence of the cross-section geometry and end support conditions on the post-buckling behavior and Direct Strength Method (DSM) design of cold-formed steel lipped channel and rack-section columns buckling and failing in distortional modes. The columns analyzed exhibit (i) four end support conditions, (ii) different cross-section dimensions and lengths, and (iii) several yield stresses. These characteristics were carefully selected in order to ensure, as much as possible, that all the columns (i) buckle and fail in "pure" distortional modes and (ii) cover a wide (distortional) slenderness range. The post-buckling equilibrium paths and ultimate loads presented and discussed in the paper were obtained through ANSYS elastic and elastic-plastic shell finite element analyses. Moreover, the ultimate strength data acquired are used to show that, regardless of the column geometry, the current DSM distortional design curve is not able to predict adequately (safely and accurately) the ultimate loads of columns with other than fixed end supports. The paper also includes a preliminary assessment/proposal of the modifications that must be incorporated into this DSM design curve in order to overcome the above limitation.

1. Introduction

Advances in fabrication versatility and low production costs have prompted the cold-formed steel industry to search for novel cross-section shapes that are structurally more efficient (higher strength-to-weight ratios), even if this goal is achieved at the expense of geometrical simplicity. Indeed, the new profiles often exhibit a quite complex geometry, in the sense that they contain a large number of walls, including end and/or intermediate stiffeners. One immediate consequence of this trend was the growing inadequacy of the methods traditionally employed to design and safety check cold-formed steel members prone to cross-section in-plane deformation, which are based on the well-known and widely accepted "effective width" concept. In particular, this method is not well suited to handle distortional buckling, an increasingly relevant instability phenomenon (i) involving a specific type of cross-section in-plane deformation, stemming from the presence of (insufficiently stiff) end stiffeners, and (ii) frequently governing the structural response and failure of members with intermediate lengths. In order to overcome the above difficulties, Schafer & Peköz (1998) proposed the Direct Strength Method (DSM), which is based on an original idea developed by Hancock *et al.* (1994) and was later considerably improved, mostly due to Schafer's efforts (2000, 2003, 2005, 2008). Because of its simplicity (it does not require any effective width calculations), rationality (incorporates the buckling behavior of the whole

[1] Civil Engineering Program, COPPE, Federal University of Rio de Janeiro, Brazil. <alandes@coc.ufrj.br>
[2] Dept. of Civil Engineering and Architecture, ICIST/IST, Technical University of Lisbon, Portugal. <dcamotim@civil.ist.utl.pt>

cross-section) and efficiency (provides safe and accurate ultimate strength estimates, on the basis of buckling and yield stresses – the former can now be readily calculated by means of easily accessible and user-friendly numerical tools), the DSM has become increasingly popular worldwide. Therefore, it is just logical that the DSM has already been included in the current versions of the North American (AISI 2007), Australian/New Zealander (AS/NZS 2005) and Brazilian (ABNT 2010) Specifications for cold-formed steel structures. It comprises separate checks against column and beam (i) global, (ii) distortional and (iii) interactive local/global failures, almost always through "Winter-type" design curves/expressions – this work deals exclusively with the DSM design against column distortional failure.

1.1 Motivation, Objective and Scope of this Work

In the course of a numerical investigation on the distortional post-buckling behavior and ultimate strength of pinned (simply supported) and fixed lipped channel and rack-section columns under fire conditions, the authors (Landesmann & Camotim 2010a,b, 2011) "accidentally" found that, for the particular column geometries considered, the accuracy of the ultimate load estimates (at room temperature) yielded by the DSM distortional design curve/expressions is quite different for pinned and fixed columns. Indeed, while the latter were predicted quite accurately, the former were clearly overestimated, particularly in the intermediate and high slenderness range[3]. This surprising finding provided the motivation for the present paper, which aims at further investigating whether the column end support conditions influence the safety and accuracy of the ultimate load estimates provided by the DSM distortional design curve/expressions.

The objective of this work is two-fold. Initially, one presents and discusses the results of a parametric study on the post-buckling and ultimate strength behaviors of lipped channel and rack-section cold-formed steel columns with various combinations of geometry and yield stress (elastic-perfectly plastic material law), and four end support conditions (fixed, pinned-fixed, pinned and fixed-free columns) – these (numerical) results are obtained from geometrically and materially non-linear shell finite element analyses carried out in ANSYS (2004). The knowledge and "exact" ultimate strength data acquired in the above parametric study are then used to assess the "quality" of the corresponding DSM distortional failure load estimates. Finally, some conclusions and recommendations are drawn from the comparison between the whole sets of numerical ("exact") distortional ultimate loads and their DSM estimates.

As mentioned before, the scope of the parametric study carried out comprises lipped channel and rack-section columns with (i) fixed (F), pinned-fixed (P-F), pinned (P) and fixed-free (F-F) end supports, (ii) a large variety of geometries (cross-section dimensions and length), all carefully selected to ensure "pure" distortional failures, (iii) a wide range distortional slenderness values (stemming from different yield stresses) and (iv) critical-mode (distortional) geometrical imperfections with small amplitudes (*10%* of the wall thickness *t*) – no residual tresses were included in the shell finite element analyses.

1.2 Outline of the Paper

The main body of the work carried out is presented in the next four sections of the paper. In order to make the issues addressed and their presentation easier to apprehend, the objectives and contents of each of these sections are briefly described and linked below:

---

[3] At this stage, it is worth noting that the calibration and validation of the DSM distortional design curve/expressions involved almost exclusively columns with rigid plates attached to their end cross-sections. Although Schafer (2000, 2005) mentions that "they were tested in the pin-pin condition", this statement is related to the column global behavior (the rigid plates usually rest on spherical hinges, knife edges or weges) – as far as the distortional behavior is concerned, the columns are fixed. Indeed, it is not easy to test columns with other than fixed end supports (*e.g.*, simply supported columns) that fail in distortional modes – it is extremely difficult to ensure that the column end sections are able to warp freely.

(i) Section 2 is devoted to the column geometry selection, achieved by means of sequences of "trial-and-error" buckling analyses. It aims at identifying column cross-section dimensions and lengths leading to, as much as possible, "pure" distortional failures and also fulfilling some additional requirements.

(ii) Section 3 begins by briefly addressing the shell finite element model employed to perform the geometrically and materially non-linear analyses, after which the numerical results concerning the column distortional post-buckling behavior and strength are presented and discussed. The elastic and elastic-plastic equilibrium paths are addressed separately and the work focuses on the influence of the column geometry and (mostly) end support conditions on the distortional post-critical strength.

(iii) Section 4 displays the ultimate strength data yielded by the parametric study and interprets them in light of the post-buckling features previously unveiled. Moreover, the trends of the numerical ultimate loads are compared with some experimental values reported in the literature.

(iv) Section 5 addresses the influence of the column end support conditions on their DSM design against distortional failure (the columns exhibiting other collapse modes are identified an excluded from this study). The comparison between the numerical and experimental ultimate load values and their estimates provided by the current DSM design curve/expressions makes it possible (iv_1) to assess how the "quality" of the latter is influenced by the end support conditions and also (iv_2) to propose preliminary ("simplistic") modifications/adjustments to take into account that influence.

2. Column Geometry Selection – Buckling Behavior

The first step in this work consisted of carefully selecting the cross-section dimensions and lengths of the lipped channel and rack-section columns to be analyzed, which exhibit four different end support conditions. At this stage, it is worth mentioning that the words "fixed", "pinned" and "free" concern the local and global displacements (including warping) and rotations – *e.g.*, a pinned end support has (i) null in-plane local displacements, global displacements and torsional rotations, and (ii) free local/global rotations and warping displacements. The selection procedure involved "trial-and-error" buckling analyses, performed with either Generalized Beam Theory (GBT) (code GBTUL – Bebiano *et al.* 2008a,b) or shell finite element analyses (ANSYS), aimed at satisfying the following requirements:

(i) Columns buckling in "pure" distortional modes and, as much as possible, also exhibiting distortional collapses. This goal is achieved by ensuring, as much as possible, that the critical buckling stress (i_1) is clearly distortional and (i_2) falls considerably below the lowest local and global bifurcation stresses.

(ii) Cross-section dimensions that are commonly used and involve different wall width proportions, namely web-to-flange width ratios. This requirement is intended to enable the assessment of whether such width proportions have a meaningful influence on the column distortional post-critical strength.

(iii) Cross-section dimensions associated with "pure" distortional failures for the four end support conditions dealt with here (only the lengths are different). Although fulfilling this requirement is by no means essential, it makes the performance of the parametric study obviously easier.

Fortunately, it was possible to fulfill all the above requirements and the end product of the "trial-and-error" selection procedure are the seven cross-section dimensions (*4* lipped channels and *3* rack-sections) given in Table 1 – note that the web-to-flange width ratio ranges from *1.0* to *2.0* (lipped channels) and from *1.0* to *1.67* (rack-sections). On the other hand, Table 2 provides, for each cross-section dimension, the corresponding four sets (one for each end support condition) of (i) a length associated with critical distortional buckling (L_D), (ii) the corresponding critical (distortional) buckling load ($P_{cr.D}$) and lowest local ($P_{b1.L}$) and global ($P_{b1.e}$) bifurcation loads, obtained with $E=210\,GPa$ (Young's modulus) and $v=0.3$ (Poisson's ratio), and (iii) the ratios between these three loads, indicating how far apart they are.

Table 1: Selected column cross-section dimensions.

Cross-section	b_1 (*mm*)	b_2 (*mm*)	b_3 (*mm*)	b_4 (*mm*)	t (*mm*)	*Area* (*cm²*)
C75	75	75	10	-	2	4.9
C100	100	50	10	-	3	6.6
C120	120	75	10	-	2.5	7.3
C130	130	100	12.5	-	2	7.1
R75	75	55	15	20	2	5.1
R100	100	100	20	20	3	11.4
R135	134.7	80.8	24.2	47.1	2.3	10.1

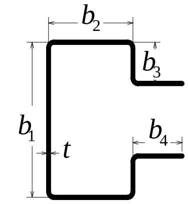

Table 2: Selected column lengths and critical/bifurcation loads.

Column	*Fixed (F)*				*Pinned-Fixed (P-F)*				*Pinned (P)*				*Fixed-Free (F-F)*			
	L_D (*cm*)	P_{cr} (*kN*)	$P_{b1.L}/P_{cr.D}$	$P_{b1.e}/P_{cr.D}$	L_D (*cm*)	P_{cr} (*kN*)	$P_{b1.L}/P_{cr.D}$	$P_{b1.e}/P_{cr.D}$	L_D (*cm*)	P_{cr} (*kN*)	$P_{b1.L}/P_{cr.D}$	$P_{b1.e}/P_{cr.D}$	L_D (*cm*)	P_{cr} (*kN*)	$P_{b1.L}/P_{cr.D}$	$P_{b1.e}/P_{cr.D}$
C75	45	212	1.37	12.87	55	147	1.95	6.40	39	128	2.21	7.11	20	84	2.53	10.4
C100	85	473	1.37	3.11	45	494	1.29	5.37	25	447	1.42	9.3	18	257	1.71	7.9
C120	88	244	1.34	9.29	90	218	1.49	5.13	38	201	1.60	15.1	25	125	1.81	14.0
C130	132	136	1.21	9.01	120	117	1.38	6.49	60	110	1.44	13.46	40	62	1.88	13.40
R75	85	295	1.31	3.94	60	241	1.52	4.95	50	193	1.88	4.35	30	129	1.98	4.53
R100	110	702	1.32	3.92	95	540	1.67	3.50	80	436	2.06	3.00	45	292	2.21	3.55
R135	242	256	1.32	3.30	180	235	1.41	3.33	94	211	1.43	6.62	60	114	1.85	7.52

One observes that the first "non-distortional" bifurcation load always corresponds to local buckling and that the ratio $P_{b1.L}/P_{cr.D}$ varies between *1.21* and *1.37* (F columns), *1.29* and *1.95* (P-F columns), *1.42* and *2.21* (P columns) and *1.71* and *2.53* (F-F columns). The first global (flexural-torsional) bifurcation load is invariably quite higher (often much higher) – indeed, the $P_{b1.e}/P_{cr.D}$ values range from *3.11* to *12.87* (F columns), *3.33* to *6.49* (P-F columns), *3.00* to *15.09* (P columns) and *3.55* to *14.0* (F-F columns). Fig. 1 illustrates the end product obtained after performing a "trial-and error" buckling analysis sequence: the curves P_{cr} vs. L (L in logarithmic scale) concerning columns exhibiting the C120 cross-section dimensions and the four end support conditions. The selected length value (L_D) is indicated on each of these and the figure includes also the four corresponding distortional critical buckling

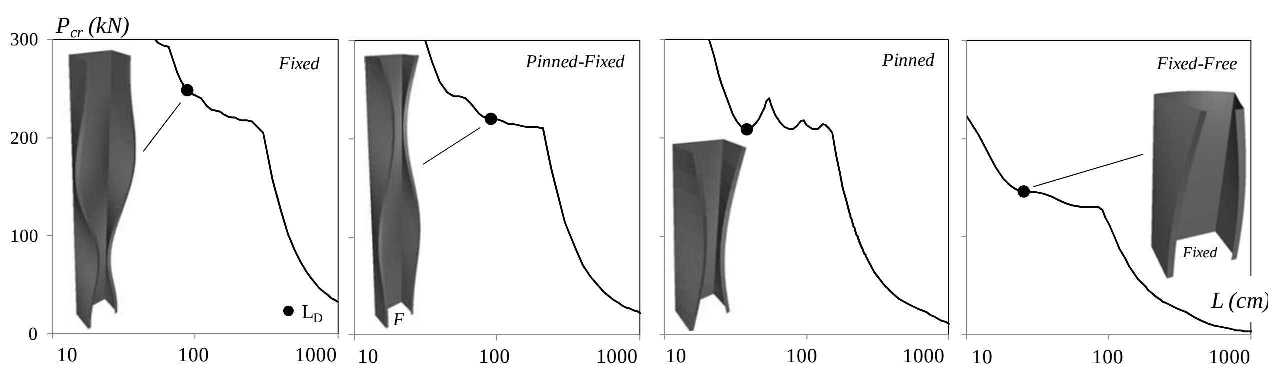

Figure 1: Curves P_{cr} vs. L concerning F, P-F, P and F-F columns with *C120* cross-section dimensions with the indication of the selected lengths (L_D) and corresponding distortional buckling mode shapes.

mode shapes[4]. Note that these mode shapes may exhibit different half-wave numbers – the general trend is that the number of half-waves increases as the end support conditions become "more restrictive" (*i.e.*, as one travels from "free" to "pinned" to "fixed").

3. Distortional Post-Buckling Behavior and Strength

After briefly addressing the numerical (shell finite element) model adopted to perform the geometrically and materially non-linear analyses, one presents and discusses results concerning the influence of the cross-section dimensions and (mostly) end support conditions on the column distortional post-buckling behavior and strength. The elastic and elastic-plastic results are addressed separately.

3.1 Numerical Model

The column distortional post-buckling equilibrium paths and ultimate strength values were determined through geometrically and materially non-linear shell finite element analyses carried out in the code ANSYS (2004). The columns were discretized into SHELL181 elements (ANSYS nomenclature – 4-node shear deformable thin-shell elements with six degrees of freedom per node and full integration) – convergence studies showed that $5\,mm \times 5\,mm$ meshes provide accurate results, while involving a reasonable computational effort. The analyses were performed by means of an incremental-iterative technique that combines Newton-Raphson's method with an arc-length control strategy. All columns exhibited (i) critical-mode (distortional) initial imperfections with small amplitudes (*10%* of the wall thickness t) and (ii) a material behavior either perfectly elastic or elastic-perfectly plastic (Prandtl-Reuss model: Von Mises yield criterion and associated flow rule), characterized by $E=210\,GPa$, $\nu=0.3$ and several yield stresses f_y[5]. No strain-hardening and/or residual tresses were included in the analyses.

The incorporation of the critical-mode initial geometrical imperfections in the columns was made automatically by means of the following procedure (*e.g.*, Dinis & Camotim 2006): (i) determination of the critical buckling mode shape, through an ANSYS shell finite element buckling analysis that adopted exactly the same discretization/mesh employed to carry out the subsequent post-buckling analysis, which was then (ii) scaled to exhibit maximum vertical displacements along the flange-stiffener longitudinal edges equal to $0.1\,t$ – this output of the buckling analysis is then "transformed" into an input of the non-linear one. Following the column distortional post-buckling asymmetry studies carried out by Prola & Camotim (2002a,b), these initial imperfections involve outward (lipped channels) and inward (rack-sections) flange-stiffener motions – those that were shown to lead to the lower post-buckling strengths[6].

Concerning the modeling of the different end support conditions, it is worth noting that:

(i) In a fixed support, the column end section was attached to a rigid plate, thus precluding the occurrence of local and global displacements and rotations, as well as warping.

(ii) In a pinned support, the membrane and bending transverse displacements of all end section nodes were prevented, while keeping the axial (warping) displacements and all the rotations free.

---

[4] Rigorously speaking, the P column curve concerns single half-wave bifurcation loads (and not critical buckling loads). However, the critical buckling loads are associated with single half-wave buckling modes up to the length selected.

[5] Note that the vast majority of the yield stresses considered in this work are unrealistically high, leading to E/f_y that largely exceed the current DSM limit for pre-qualified columns ($E/f_y=340$). The reason for selecting such high yield stresses was to make it possible to analyze columns with high slenderness values, thus covering a wide slenderness range.

[6] Obviously, the distinction between outward and inward flange-stiffener motions is only relevant when the column critical buckling mode involves an odd number of half-waves – in this case, it is assumed in this work that the buckling mode nature is governed by that associated with the higher number of half-waves (outward or inward).

(iii) In a free end, all local and global displacements and rotations may occur freely.

(iv) To enable the load application, the rigid-body axial translation is free at one or both end sections.

The axial compression is applied by means of either (i) set of concentrated forces acting on the nodes of a pinned or free end section or (ii) a concentrated force applied on the rigid plate point corresponding to a fixed end section centroid. The above forces are always increased in small increments, by means of the ANSYS automatic load stepping procedure.

3.2 Elastic Post-Buckling Behavior

In order to assess the qualitative and quantitative influence of the end support conditions on the column elastic distortional post-buckling behavior, Figs. 2 and 3 show the post-buckling equilibrium paths of columns exhibiting C130 and R135 cross-sections and exhibiting the four end support combinations dealt with in this work. These equilibrium paths plot the applied load real value (Fig. 2) or normalized value with respect to the corresponding column critical buckling load $P_{cr.D}$ (Fig. 3) versus the normalized displacement $|\delta|/t$, where $|\delta|$ is the absolute value of the maximum vertical displacement occurring along the flange-stiffener longitudinal edges and t is the wall thickness. The observation of these four sets of four distortional post-buckling equilibrium paths prompts the following remarks:

(i) As it would be logical to expect, the real post-buckling strength decreases as one travels along the column end support condition sequence F, P-F, P and F-F.

(ii) At least for these particular column geometries, the lipped channel column real post-buckling strengths are higher than their rack-section counterparts. Moreover, the real strength differences associated with the various end support conditions are also are higher for the lipped channel columns.

(iii) The picture changes when the normalized post-buckling strengths are considered. Indeed, although they are still higher for the F columns, the values concerning the P-F, P and F-F columns are very close and can be viewed as shared by all of them (C130 and R135 columns). The lipped channel column normalized post-buckling strengths are again higher than their rack-section counterparts.

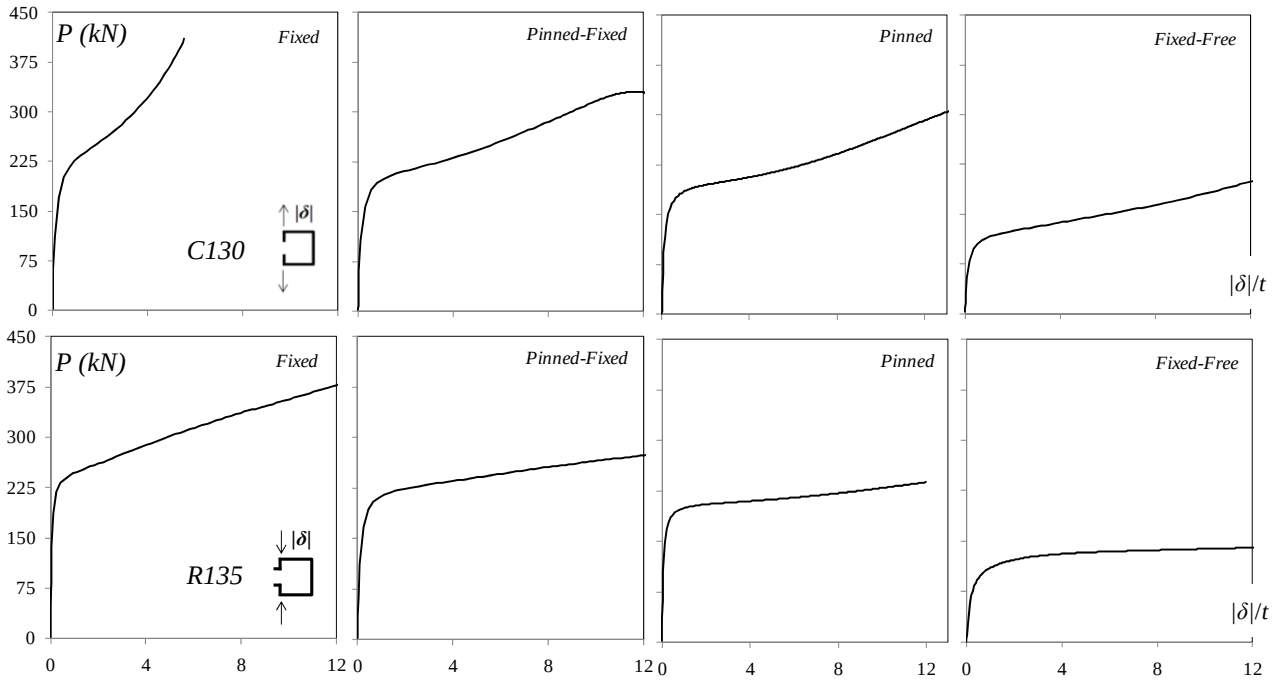

Figure 2: Elastic equilibrium paths *P vs.* $|\delta|/t$ for C130 and R135 columns with F, P-F, P and F-F end support conditions.

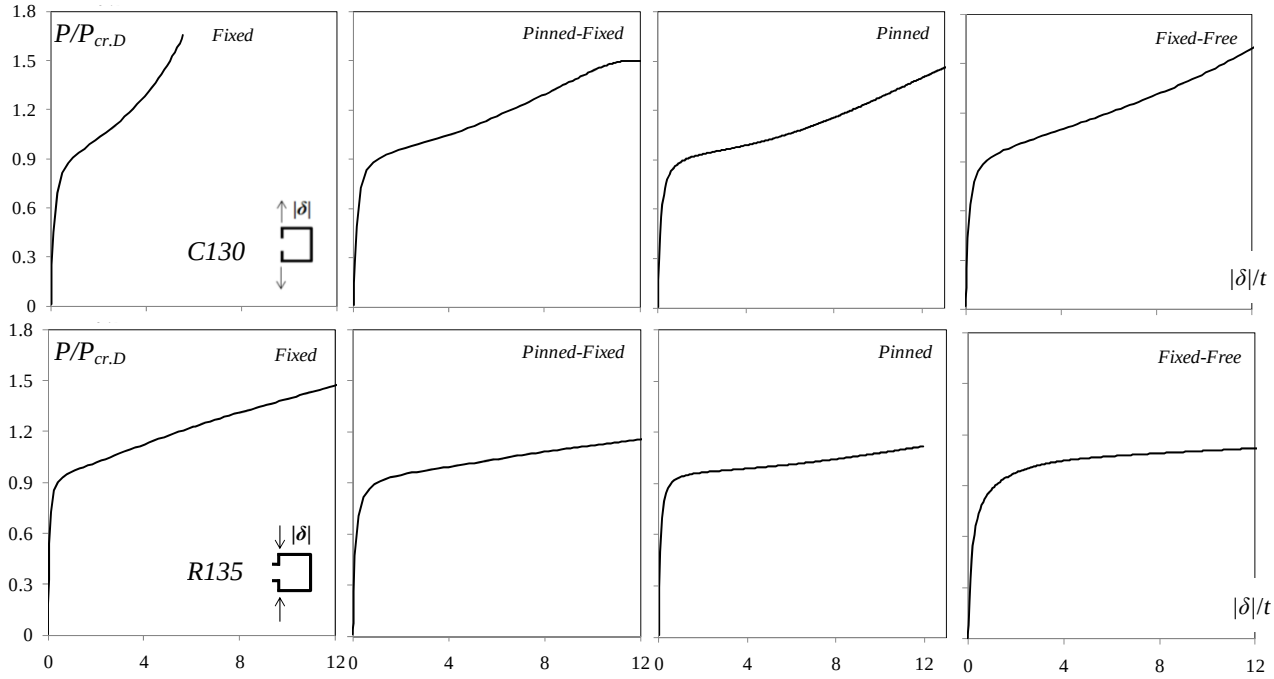

Figure 3: Normalized elastic equilibrium paths $P/P_{cr.D}$ *vs.* $|\delta|/t$ for the same F, P-F, P and F-F C130 and R135 columns.

3.3 Elastic-Plastic Post-Buckling Behavior – Ultimate Strength

Attention is now devoted to the qualitative and quantitative influence of the end support conditions on the column elastic-plastic distortional post-buckling and ultimate strength behavior. In order to achieve a more meaningful comparison, all the post-buckling results presented and discussed in this section concern columns with different geometries (cross-section shape and dimensions, and lengths), but sharing exactly the same distortional slenderness $\overline{\lambda}_D=(f_y/\sigma_{cr.D})^{0.5}=2.358$ (a fairly high value) – this common slenderness is ensured by properly selecting "custom made" yield stresses[7]. Table 3 shows, for each end support condition, the column (i) geometries and critical (distortional) buckling loads $P_{cr.D}$, already presented in Tables 1 and 2, (ii) ultimate loads P_u, obtained from ANSYS second-order elastic-plastic shell finite element analyses, and (iii) ultimate load ratios $P_u/P_{cr.D}$, together with the corresponding means and standard deviations, which provide post-critical strength reserve estimates. In order to enable a better visualization of the differences between the ultimate load ratios concerning the four end support conditions, Fig. 4 plots all the $P_u/P_{cr.D}$ values side by side. Finally, Fig. 5 displays, for each end support condition, a sample of the non-linear (geometrically and materially) equilibrium paths P/P_{cr} *vs.* $|\delta|/t$ determined to obtain the ultimate loads P_u (identified by white circles) – these equilibrium paths concern lipped channel (C120) and rack-section (R100) columns and most of them are only shown up to collapse[8]. Finally, Fig. 6 depicts the column deformed configurations occurring in the close vicinity of the limit points of each equilibrium path displayed in Fig. 5 – they provide fairly accurate representations of the (distortional) failure modes exhibited by the corresponding lipped channel and rack-section columns.

After observing the elastic-plastic distortional post-buckling and ultimate strength results presented in Table 3 and Figs. 4 to 6, the following conclusions can be drawn:

---

[7] As mentioned earlier, most of the yield stresses selected to meet this "common slenderness criterion" is unrealistically high.

[8] It is worth pointing out that numerical difficulties sometimes prevented an adequate determination of the equilibrium path descending branches (see Fig. 5). Nevertheless, it was carefully ensured that the $P_u/P_{cr.D}$ values presented in Table 3 are based on accurate estimates of the real column ultimate loads.

(i) First of all, one notices that there is a considerable scatter of the $P_u/P_{cr.D}$ values within columns sharing the same end support conditions. Indeed, these values vary between *1.84* and *1.30* (F – average and standard deviation equal to *1.58* and 0.*19*), *1.33* and *1.10* (P-F – average and standard deviation equal to *1.20* and 0.*09*), *1.31* and *1.01* (P – average and standard deviation equal to *1.14* and 0.*11*) and *1.16* and *0.91* (F-F – average and standard deviation equal to *1.06* and 0.*11*) – Fig. 4 provides a pictorial representation of these $P_u/P_{cr.D}$ scatters. This dispersion may be attributed to the wide variety of column geometries considered in this study. Indeed, besides the two cross-

Table 3: Geometries, buckling loads, ultimate loads and ultimate load ratios for F, P-F, P and F-F columns with $\overline{\lambda}_D$=*2.358*.

Column	*Fixed (F)*			*Pinned-Fixed (P-F)*			*Pinned (P)*			*Fixed-Free (F-F)*		
	$P_{cr.D}$ *(kN)*	f_y *(MPa)*	$\frac{P_u}{P_{cr.D}}$	$P_{cr.D}$ *(kN)*	f_y *(MPa)*	$\frac{P_u}{P_{cr.D}}$	$P_{cr.D}$ *(kN)*	f_y *(MPa)*	$\frac{P_u}{P_{cr.D}}$	$P_{cr.D}$ *(kN)*	f_y *(MPa)*	$\frac{P_u}{P_{cr.D}}$
C75	212	2404	1.84	147	1663	1.10	128	1455	1.01	84	948	1.11
C100	473	3988	1.72	494	4163	1.33	447	3765	1.31	257	2170	1.13
C120	244	1874	1.63	218	1669	1.18	201	1544	1.23	125	962	1.16
C130	136	1065	1.67	117	918	1.11	110	862	1.02	62	488	1.16
R75	295	3216	1.35	241	2624	1.29	193	2110	1.13	129	1411	0.94
R100	702	3425	1.30	540	2635	1.19	436	2125	1.09	292	1423	0.91
R135	256	1412	1.55	235	1295	1.22	211	1164	1.21	114	630	0.99
Mean			1.58			1.20			1.14			1.06
S.D			0.19			0.09			0.11			0.11

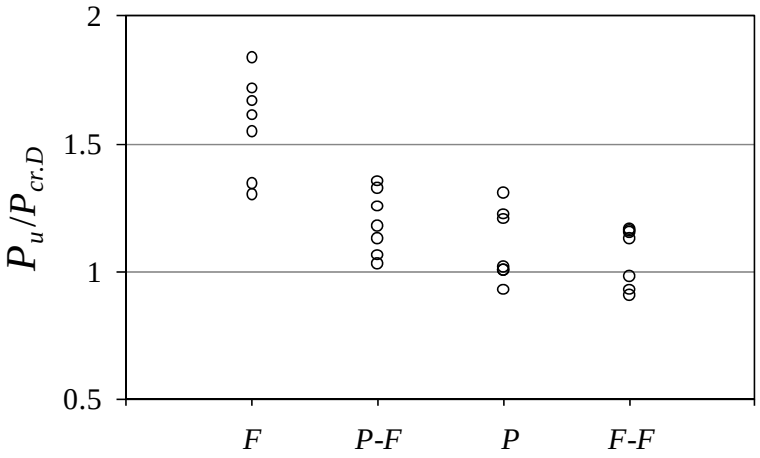

Figure 4: $P_u/P_{cr.D}$ values concerning columns with the four end support conditions considered.

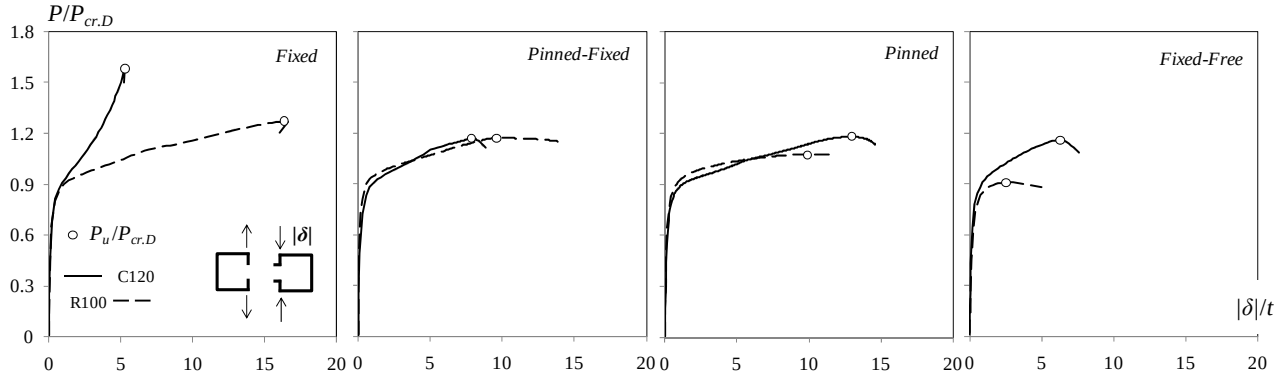

Figure 5: Elastic-plastic distortional equilibrium paths (P/P_{cr} *vs.* $|\delta|/t$) concerning F, P-F, P and F-F C120 and R100 columns.

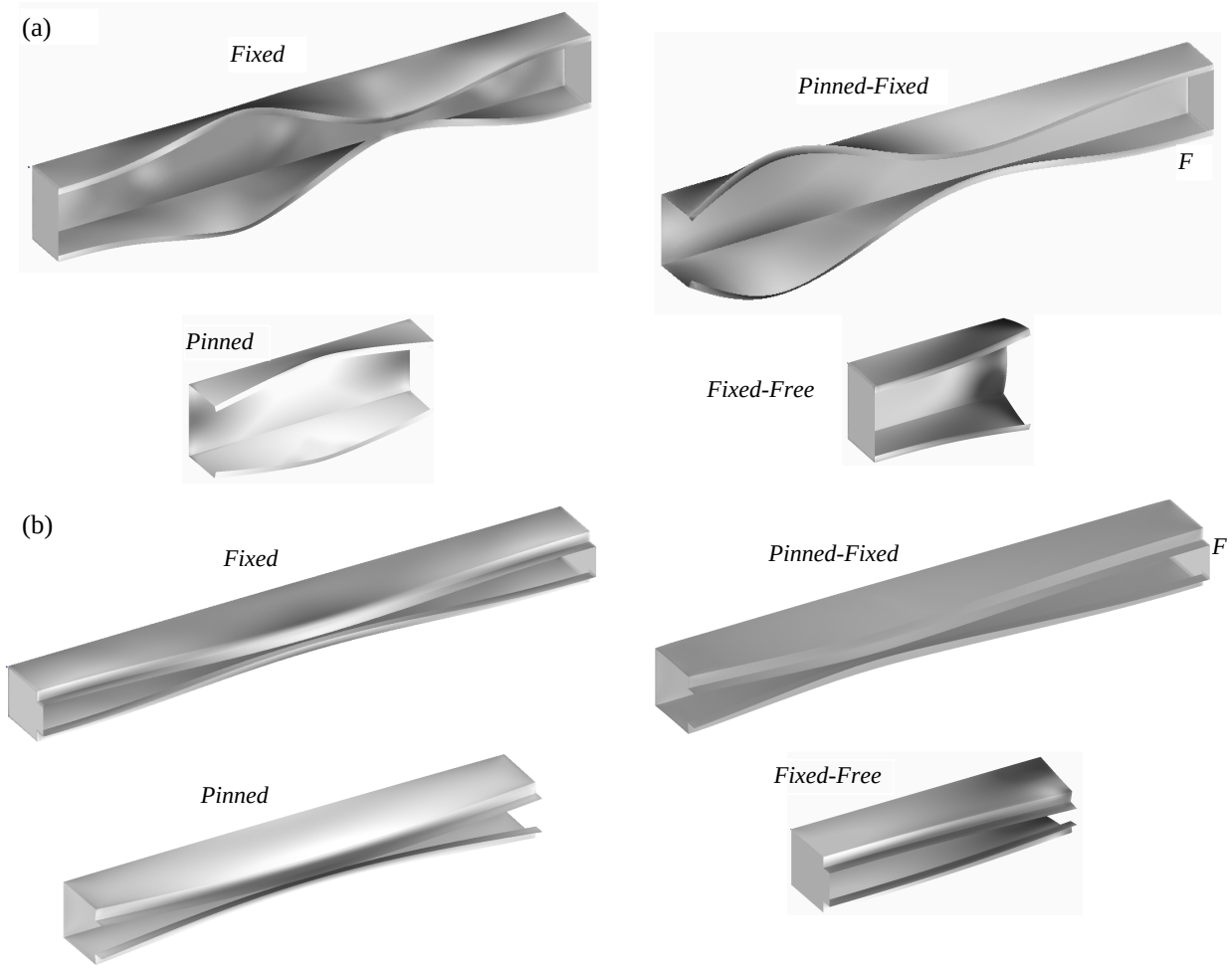

Figure 6: Distortional failure modes concerning the F, P-F, P and F-F (a) C120 and (b) R100 columns.

section shapes, the columns analyzed exhibit quite different combinations of length and cross-section dimensions. Most likely, this fact has strong implications on the corresponding column distortional post-buckling strengths (elastic or elastic-plastic)[9] – *e.g.*, note the marked differences between the equilibrium paths concerning the C120 and R100 F and F-F columns, which are presented in Fig. 5. Moreover, Fig. 5 further shows that the ductility prior to failure also varies considerably between these two column pairs.

(ii) Regardless of the geometry, the $P_u/P_{cr.D}$ values concerning the lipped channel F columns are considerably higher than their P-F, P and F-F counterparts. The differences with respect to the highest of the remaining three, which may be either of them, are: *73%* (C75 – F-F), *39%* (C100 – P-F), *40%* (C120 – P) and *51%* (C130 – F-F). In rack-section columns, the picture quite different: (ii_1) the $P_u/P_{cr.D}$ values are ordered according to the sequence F, P-F, P, F-F and (ii_2) the decreases between the F and P-F values are much smaller – *6%* (R75), *11%* (R100) and *33%* (R135).

(iii) Generally speaking, it seems fair to say that the F column $P_u/P_{cr.D}$ values are one order of magnitude above those associated with the other columns – indeed, the lowest F column value (*1.30*) is almost

[9] The authors are not aware of any existing work on the variation of the column distortional post-buckling strength with its geometry (cross-section shape, cross-section dimensions and length). In view of the results reported in this paper, it was decided to investigate this issue in the near future and, moreover, to assess also the role played by the column end support conditions in the above variation – hopefully, the outcome of such investigation will be available fairly soon.

identical to highest value concerning the remaining end support conditions (*1.33*).

(iv) While the P-F and P column $P_u/P_{cr.D}$ values are fairly similar (even if the latter are slightly below the former), those concerning the F-F columns fall visibly below. Nevertheless, the differences are much smaller than the ones separating the F columns from their F-P and P counterparts – see Fig. 4.

(v) While the collapse modes of the C120 and R100 P-F, P and F-F columns are clearly distortional, the two F columns fail in modes that exhibit a certain amount of local/distortional interaction. Indeed, local deformations involving several half-waves are visible in the web – see Figs. 7(a)-(b), providing "rear views" of the C120 and R100 F columns. This fact is not surprising, if one realizes that the F column collapse loads ($P_u/P_{cr.D}$=*1.63*; *1.30*) either considerably exceed (C120) or are extremely close to (R100) their critical local bifurcation loads ($P_{b1.L}/P_{cr.D}$=*1.34*; *1.32* – see Table 2)[10].

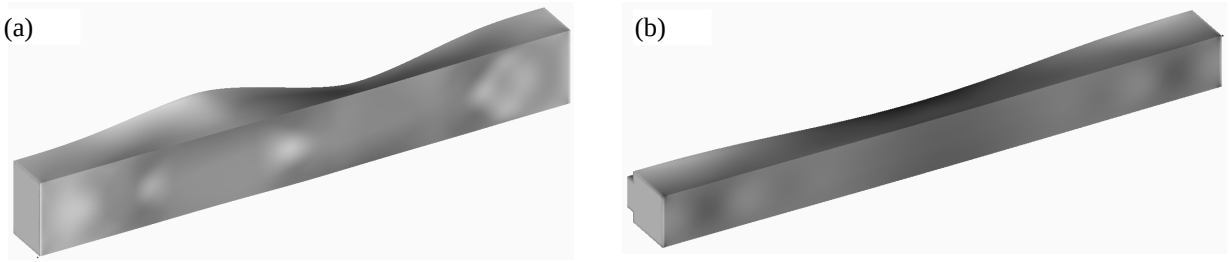

Figure 7: (a) C120 and (b) R100 F column failure mode rear views: evidence of local deformations (local/distortional interaction).

4. Ultimate Strength Data

The aim of this section is to present and discuss the ultimate strength data gathered from the parametric study carried out, which involved a total of *168* columns, corresponding to all possible combinations of (i) the seven column geometries defined in Tables 1 and 2, (ii) the four end support conditions dealt with in this work and (iii) the six yield stresses (f_y=*250-550-700-1200-1600-2000 MPa*), selected to enable covering wide distortional slenderness ranges for all column sets: $\overline{\lambda}_D$ varies between *0.57* and *3.22* (F columns), *0.57* and *3.44* (P-F columns), *0.60* and *3.59* (P columns) and *0.8* and *4.77* (F-F columns). Tables A1 to A4, presented in the Annex of this paper, contain all the numerically obtained column ultimate loads (P_u), normalized with respect to the corresponding squash loads (P_y=Af_y), and associated distortional slenderness values ($\overline{\lambda}_D$). Those four sets of values (one for each end support condition) are also plotted in Fig. 8, together with a number of available experimental results obtained by several researchers, which were extracted from Schafer's recent state-of-the-art report (2008)[11]. The observation of these four plots prompts the following remarks:

(i) As it would be logical to expect, the four $P_u/P_{cr.D}$ *vs.* $\overline{\lambda}_D$ "clouds" follow trends that can be accurately described by "Winter-type" design curves. Moreover, the "vertical dispersion" is acceptable in all of them, even if it is a bit high for the slender F-F columns.

(ii) It is clear that the F column numerical $P_u/P_{cr.D}$ values are well above those concerning the other (P-F, P and F-F) columns. The "dashed grid lines" included in Fig. 8, corresponding to $\overline{\lambda}_D$ =*1.5* and $\overline{\lambda}_D$=*2.5*, provide a better visualization of this fact – the F column horizontal lines lie visibly above

[10] Note that local/distortional interaction also occurs in other F and P-F columns, whenever (i) $P_{b1.L}/P_{cr.D}$ is not significantly larger than *1.0* and (ii) the yield stress is high enough to enable the "interference" of local buckling prior to collapse. Such columns are identified in Tables A1 to A4, presented in the Annex.

[11] As mentioned earlier, all these experimental results concern columns with rigid plates attached to their end cross-sections, thus meaning that they are distortionally fixed (regardless of how those rigid plates are supported, which only affects the column global end support conditions).

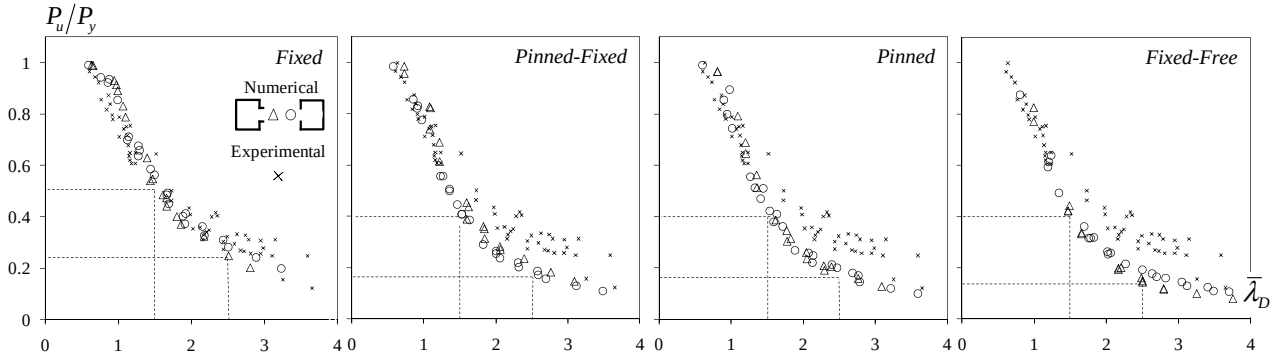

Figure 8: Numerical (F, P-F, P and F-F columns) and experimental (F columns – Schafer 2008) ultimate load ratios $P_u/P_{cr.D}$ plotted against the column distortional slenderness $\overline{\lambda}_D$.

their P-F, P and F-F column counterparts (which are located roughly at the same level). Moreover, it is also clear that the experimental results, all involving F columns, are much closer to the F column numerical $P_u/P_{cr.D}$ values.

(iii) At first sight, the $P_u/P_{cr.D}$ *vs.* $\overline{\lambda}_D$ "clouds" concerning the P-F, P and F-F columns are quite similar (and also similarly apart from the experimental results). However, a closer look reveals that there are non-negligible differences between the F-F lipped channel and rack-section slender column $P_u/P_{cr.D}$ values – the latter are consistently lower than the former[12].

5. DSM Design Considerations

This section addresses the applicability of the Direct Strength Method (DSM) to estimate the ultimate strength of columns failing in distortional modes and exhibiting various end support conditions, namely the lipped channel and rack-section numerically analyzed in this work. First of all, it is worth mentioning that a DSM column ultimate strength estimate is the minimum of three nominal loads, concerning global ($P_{n.e}$), distortional ($P_{n.D}$) and interactive local/global ($P_{n.Le}$) collapses – *i.e.*, $P_{u.DSM}=min\{P_{n.e},P_{n.D},P_{n.Le}\}$[13]. These nominal loads are obtained by means of the expressions (design curves)

$$P_{n.e}=\begin{cases}\left(0.658^{\overline{\lambda}_e^2}\right)P_y & \text{for } \overline{\lambda}_e \le 1.5\\ \left(0.877/\overline{\lambda}_e^2\right)P_y & \text{for } \overline{\lambda}_e \le 1.5\end{cases} \quad (1)$$

$$P_{n.D}=\begin{cases}P_y & \text{for } \overline{\lambda}_D \le 0.561\\ \left[1-0.25\left(P_{cr.D}/P_y\right)^{0.6}\right]\left(P_{cr.D}/P_y\right)^{0.6}P_y & \text{for } \overline{\lambda}_D > 0.561\end{cases} \quad (2)$$

$$P_{n.Le}=\begin{cases}P_{n.e} & \text{for } \overline{\lambda}_{Le} \le 0.776\\ \left[1-0.15\left(P_{cr.L}/P_{n.e}\right)^{0.4}\right]\left(P_{cr.L}/P_{n.e}\right)^{0.4}P_{n.e} & \text{for } \overline{\lambda}_{Le} > 0.776\end{cases}, \quad (3)$$

[12] Although to a smaller extent, the same also occurs for the P columns. Only the P-F lipped channel and rack-section column $P_u/P_{cr.D}$ are "well mixed together".

[13] Since the column critical buckling and failure modes do not always exhibit the same nature (although they often do), it is necessary to check for the three collapse mechanisms, regardless of the critical buckling mode nature. For instance, a column may have a distortional critical buckling mode and fail in a global mode, which is associated with a lower post-critical strength, provided that the distortional and global critical buckling loads are not too far apart.

where (i) P_y is the column squash load and (ii) $\overline{\lambda}_e=(P_y/P_{cr.e})^{0.5}$, $\overline{\lambda}_D=(P_y/P_{cr.D})^{0.5}$ and $\overline{\lambda}_{Le}=(P_{n.e}/P_{cr.L})^{0.5}$ stand for the global, distortional and interactive local/global slenderness.

The first step consists of computing $P_{n.e}$, $P_{n.D}$ and $P_{n.Le}$ for the *168* columns dealt with in this investigation, in order to assess the nature of the column collapse predicted by the DSM – all these nominal loads, together with the corresponding slenderness values, are presented in Tables A1 (F columns), A2 (P-F columns), A3 (P columns) and A4 (F-F columns). It was found that, for seven columns, $P_{u.DSM}=P_{n.Le}$, which means that they are predicted to exhibit interactive local/global collapses. However, the subsequent inspection of the numerical failure modes of all these columns did not confirm this prediction, as no trace of global deformations was detected – instead, these failure modes either involve only distortional deformations (*3* C100 columns) or combine local and distortional deformations (*4* R135 columns). In order to illustrate this statement, Figs. 9(a)-(d) shows the collapse modes of four of these columns, namely (i) C100 P-F and P columns ($\overline{\lambda}_D=0.58$ and $\overline{\lambda}_D=0.61$) and (ii) R135 F and P-F columns ($\overline{\lambda}_D=2.81$ and $\overline{\lambda}_D=2.93$), providing clear evidence of their distortional and local/distortional interactive natures. All the seven columns with $P_{u.DSM}=P_{n.Le}$ are identified in Tables A1 to A4 by an asterisk next to the $P_{u.DSM}$ value.

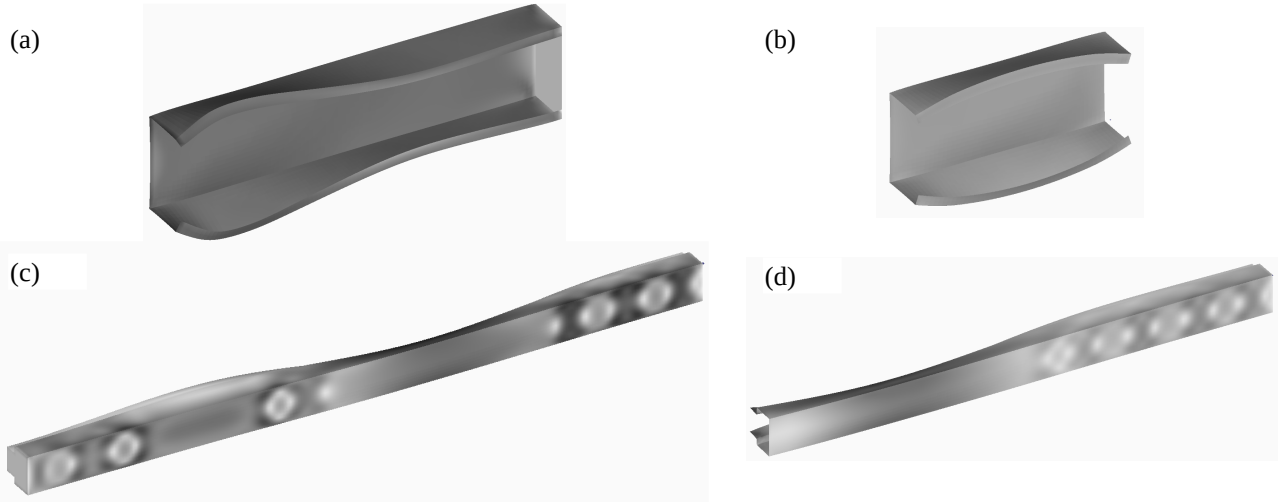

Figure 9: (a) C100 P-F ($\overline{\lambda}_D=0.58 - P_{n.D}/P_{n.Le}=1.01$), (b) C100 P ($\overline{\lambda}_D=0.61 - P_{n.D}/P_{nLe}=1.03$), (c) R135 F ($\overline{\lambda}_D=2.81 - P_{nD}/P_{nLe}=1.13$) and (d) R135 P-F ($\overline{\lambda}_D=2.93 - P_{nD}/P_{nLe}=1.14$) column distortional and interactive local/distortional failure modes.

Moreover, the numerical collapse modes of all columns with $P_{b1.L}/P_{cr.D}$ not significantly larger than *1.0* (the condition $P_{b1.L}/P_{cr.D}<2.0$ was adopted) were inspected to look for evidence of local/distortional mode interaction (see Figs. 7(a)-(b) or 9(c)-(d)). Whenever such evidence was found, the columns are identified in Tables A1 to A4 as exhibiting "L+D failures". These columns were also included in the present investigation, since they collapse in predominantly distortional modes, but their DSM ultimate strength predictions will be specifically addressed ahead in the paper. It is still worth noting that only F and P-F columns with $P_{b1.L}/P_{cr.D}\leq 1.52$ exhibited "L+D failures" – moreover, the corresponding $P_u/P_{b1.L}$ values are always higher than *0.81* (for both the F and P-F columns)[14].

Fig. 10 compares the current DSM distortional design curve with (i) the numerically obtained ultimate loads, concerning the analyzed F, P-F, P and F-F columns that buckle in distortional modes and exhibit either distortional or interactive local/distortional collapses (*42* columns per end support condition), and

[14] Although there are also P columns with $P_{b1.L}/P_{cr.D}<1.52$ and $P_u/P_{b1.L}>0.81$ (up to 0.90), no evidence of local/distortional interaction was detected in their ANSYS failure modes.

(ii) the experimental ultimate strength values reported by Schafer (2008), concerning only F columns. Fig. 11, on the other hand, shows the corresponding $P_{n.D}/P_u$ vs. $\overline{\lambda}_D$ plots (values given in Tables A1 to A4), thus providing pictorial representations of the accuracy and safety of the DSM ultimate strength estimates. In both figures, the F and P-F columns whose failure modes exhibit local/distortional interaction are identified by "grey circles/triangles". The observation of these four pairs of figures prompts the following remarks:

(i) Obviously, the DSM design curve provides accurate and mostly safe predictions of the experimental distortional loads. Moreover, it also predicts similarly well the F column numerical ultimate strengths, as attested by the corresponding $P_{n.D}/P_u$ values, given in Table A1 and plotted in Fig. 11 – their with average, standard deviation, maximum and minimum values are *0.99*, *0.10*, *1.33* and *0.84*.

(ii) There are a fair number of F columns experiencing some degree of local/distortional interaction at collapse, which naturally exhibit high $\overline{\lambda}_D$ values – the yield stress is high enough to enable the "interference" of the local mode along the distortional post-buckling equilibrium path. However, the "quality" of the associated DSM ultimate load predictions remains quite good, perfectly in line with those concerning the experimental results. At this stage, it is worth mentioning that it has been shown, in the context of lipped channel F columns, that the ultimate strength erosion stemming from local/distortional interaction may be quite meaningful in the high distortional slenderness range, thus requiring the development of a novel DSM design curve to account for this phenomenon (*e.g.*, Kwon *et al.* 2009 and Silvestre *et al.* 2009a). However, it was also recently found that the local/distortional interaction effects are considerably larger when the ratio between the critical local and distortional buckling loads is equal or below (and not too far apart) *1.0* (Dinis *et al.* 2009, Silvestre *et al.* 2009b and Young *et al.* 2009). Since this ratio varies from *1.21* to *1.37* in the F columns analyzed here, it is not surprising that their ultimate loads are well estimated by the DSM distortional design curve.

(iii) Although there are no published results (at least to the authors' best knowledge) concerning the

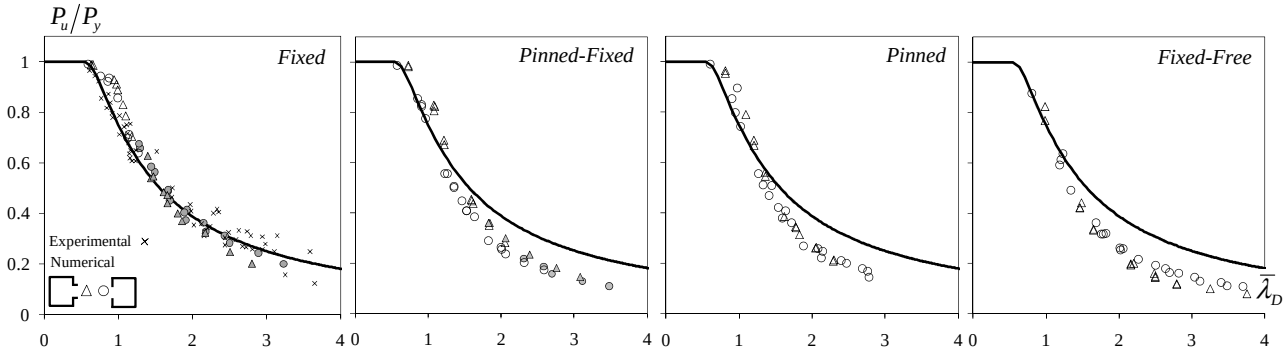

Figure 10: Comparison between the DSM distortional curve and the F, P-F, P and F-F column ultimate loads.

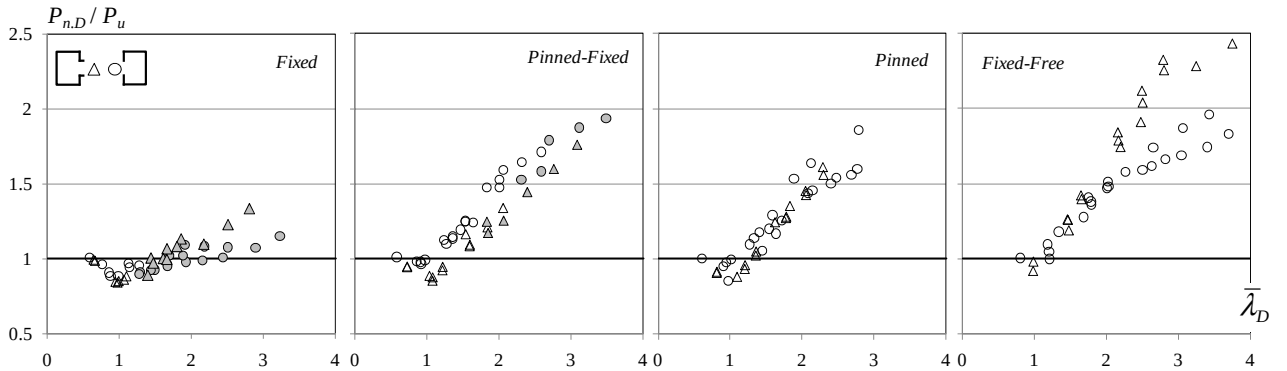

Figure 11: $P_{n.D}/P_u$ ratio values concerning the F, P-F, P and F-F columns plotted against the distortional slenderness $\overline{\lambda}_D$.

post-buckling and ultimate strength behavior of P-F columns affected by local/distortional coupling, it will be assumed here that the interaction effects are qualitatively similar to those unveiled for the F columns. Moreover, the P-F column plot in Fig.10 shows that the grey and white circles/triangles are well "mingled" together, which means that the ultimate loads with and without local/distortional interaction follow exactly the same trend ("Winter-type curve").

(iv) Concerning the P-F, P and F-F columns, it is readily observed that their ultimate strength excessively overestimated by the DSM design curve in the high slenderness range ($\overline{\lambda}_D \geq 1.5$). Indeed, accurate (safe or unsafe) predictions only occur for low and moderate slenderness values.

(v) The $P_{n.D}/P_u$ "distributions", displayed in Fig. 11, are quite similar for all the P-F and P columns and the lipped channel F-F columns. Concerning the rack-section F-F columns, their $P_{n.D}/P_u$ values either (v_1) "mingle" quite well with the above "distributions", for $\overline{\lambda}_D \leq 2.0$, or ($v_2$) lie considerably above them, for the higher slenderness values ($\overline{\lambda}_D > 2.0$).

(vi) The averages, standard deviations, maximum and minimum values of the $P_{n.D}/P_u$ values concerning the "non-F" columns are (vi_1) *1.27, 0.30, 1.94, 0.85* (P-F columns), (vi_2) *1.32, 0.32, 2.02, 0.85* (P columns) and (vi_3) *1.62, 0.42, 2.53, 0.92* (F-F columns).

(vii) In view of the above facts, it is clear that the significant differences between the (vii_1) F and (vii_2) P-F, P and F-F column distortional post-critical strengths are not adequately reflected in their (distortional) critical buckling stresses. Therefore, it is necessary to consider different DSM design curves to predict efficiently the distortional failure loads of column with the latter end support conditions. On the basis of the results of the limited parametric study carried out in this work, it seems that a single additional design curve will be capable of predicting adequately the ultimate strength of the lipped channel and rack-section P-F and P columns and lipped channel F-F columns. However, such a curve overestimates the most slender rack-section F-F column ultimate loads by non-negligible amounts.

5.1 Proposal of an Additional Design Curve

Guided by the ultimate strength data acquired though the limited parametric study carried out in this work, it is possible to propose an additional DSM design curve that only modifies the current one for fairly high slenderness values, while retaining the accuracy and safety of its predictions for the less slender columns. Although it was found that the more slender rack-section F-F column $P_{n.D}/P_u$ values are considerably higher than the remaining ones, simplicity reasons lead to search for a single design curve covering all P-F, P and F-F columns. The outcome of this effort is the modified design curve defined by the expressions

$$P^*_{n.D} = \begin{cases} P_y & \text{for } \bar{\lambda}_D \leq 0.561 \\ \left[1 - 0.25\left(P_{cr.D}/P_y\right)^{0.6}\right]\left(P_{cr.D}/P_y\right)^{0.6} P_y & \text{for } 0.561 < \bar{\lambda}_D \leq 1.188 \\ \left[0.55 + 0.4\left(P_{cr.D}/P_y\right)^{0.8}\right]\left(P_{cr.D}/P_y\right)^{0.8} P_y & \text{for } \bar{\lambda}_D > 1.188 \end{cases} \quad (4)$$

only differs from the current ones for $\overline{\lambda}_D \geq 1.188$. Fig. 12 compares this (proposed) design curve with the numerical ultimate loads, concerning the P-F, P and F-F columns considered earlier. On the other hand, the $P^*_{n.D}/P_u$ values are given in Table A5, presented in Annex, and the corresponding $P^*_{n.D}/P_u$ vs. $\overline{\lambda}_D$ plots are shown in Fig. 13. After observing these three pairs of figures, the following comments are appropriate:

(i) The averages, standard deviations, maximum and minimum values of the $P^*_{n.D}/P_u$ ratio concerning the "non-F" columns are (i_1) *0.87, 0.09, 1.08* and *0.71* (P-F columns), (i_2) *0.86, 0.08, 1.01* and *0.72* (P columns) and (i_3) *0.89, 0.11, 1.09, 0.66* (F-F columns).

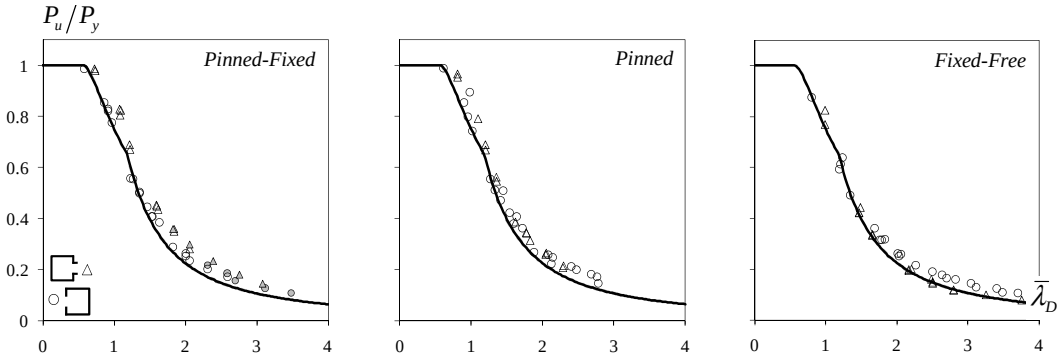

Figure 12: Comparison between the modified DSM design curve and the P-F, P and F-F column ultimate loads.

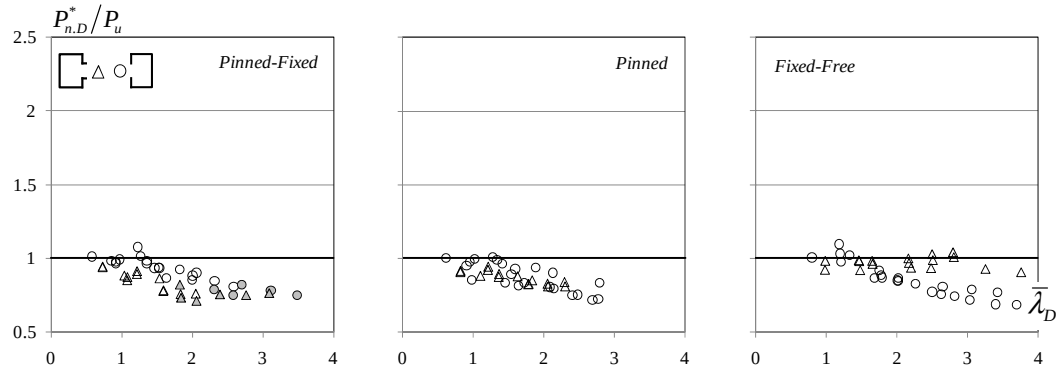

Figure 13: $P^*_{n.D}/P_u$ ratio values concerning the P-F, P and F-F columns plotted against the distortional slenderness $\overline{\lambda}_D$.

(ii) In order to avoid unsafe ultimate load estimates for a few very slender ($\overline{\lambda}_D > 2.0$) rack-section F-F columns, the proposed design curve clearly underestimates all the remaining slender ($\overline{\lambda}_D \geq 1.5$) columns: (ii$_1$) lipped channel F-P, P and F-F columns and (ii$_2$) rack-section F-P and P columns.

(iii) If only F-P and P columns are considered, it is possible to propose a more accurate design curve – such an alternative modified design curve is defined by the expressions

$$P^{**}_{n.D} = \begin{cases} P_y & \text{for } \overline{\lambda}_D \leq 0.561 \\ \left[1 - 0.25\left(P_{cr.D}/P_y\right)^{0.6}\right]\left(P_{cr.D}/P_y\right)^{0.6} P_y & \text{for } 0.561 < \overline{\lambda}_D \leq 1.133 \\ \left[0.65 + 0.2\left(P_{cr.D}/P_y\right)^{0.75}\right]\left(P_{cr.D}/P_y\right)^{0.75} P_y & \text{for } \overline{\lambda}_D > 1.133 \end{cases} \quad (5)$$

Figs. 14(a)-(b) compare this alternative proposed design curve with the numerical ultimate loads, concerning the P-F and P columns previously dealt with. As for the $P^{**}_{n.D}/P_u$ values, also given in Table A5, they are plotted against $\overline{\lambda}_D$ in Figs. 14(c)-(d). One readily observes that:

(iii.1) The averages, standard deviations, maximum and minimum values of the $P^{**}_{n.D}/P_u$ values now become (iii$_1$) *0.94*, *0.06*, *1.05*, *0.81* (P-F columns) and (iii$_2$) *0.94*, *0.05*, *1.05*, *0.85* (P columns), which confirms the improved "quality" of the estimates provided by the alternative modified design curve.

(iii.2) If the very slender ($\overline{\lambda}_D > 2.0$) rack-section columns are excluded, the alternative modified design curve also estimates quite well the F-F column ultimate loads. The corresponding average, standard deviation, maximum and minimum values of the $P^{**}_{n.D}/P_u$ ratios read *0.96*, *0.05*, *1.05*, *0.87 – i.e.*, the "quality indicators" of the estimates are similar to (or even slightly better than) those associated with the P-F and F columns (see the previous item).

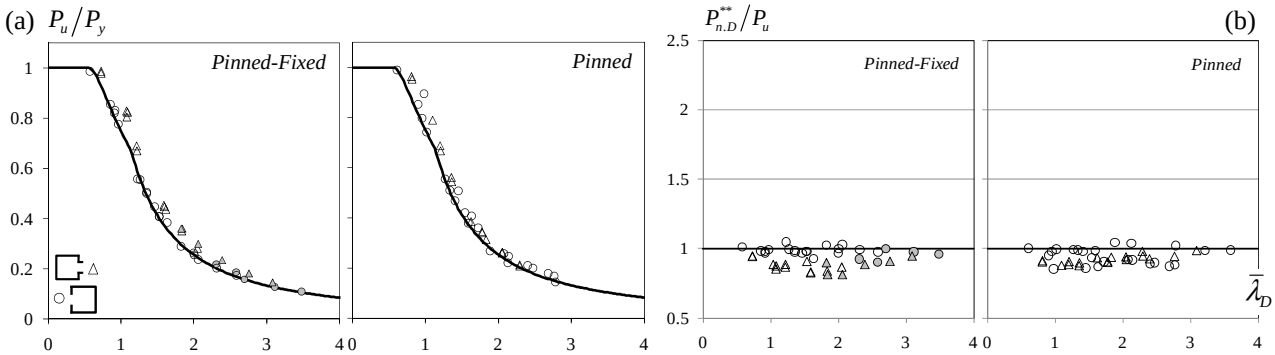

Figure 14: (a) Comparison between the second modified DSM design curve and the P-F and P column ultimate loads, and (b) corresponding $P^{**}_{n.D}/P_u$ ratio values plotted against the distortional slenderness $\overline{\lambda}_D$.

Finally, Fig. 15 summarizes the work carried out and makes it possible to compare the three proposed distortional design curves: (i) Eq. (2), for the F columns (current DSM design curve), (ii) Eq. (5), for the P-F and P columns, and (iii) Eq. (4), for the F-F columns – recall that, if the very slender ($\overline{\lambda}_D > 2.0$) rack-section columns are excluded, Eq. (5) is also applicable to the F-F columns.

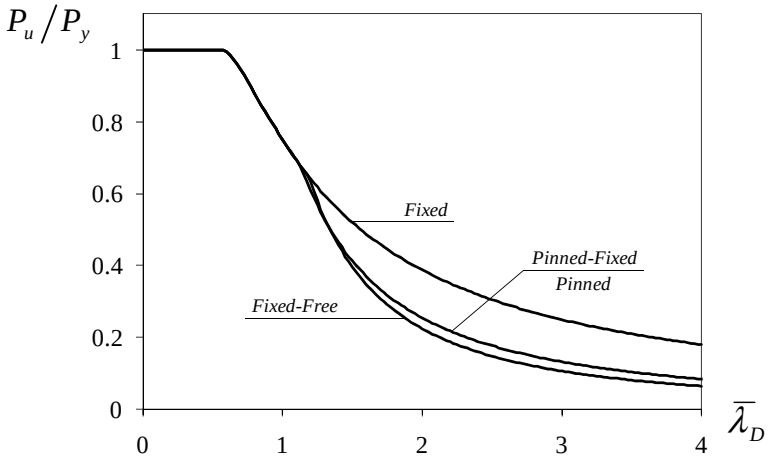

Figure 15: Comparison between the current DSM design curve and the two modifications proposed in this work.

6. Conclusion

This paper reported a numerical (ANSYS shell finite element analysis) investigation on the influence of the cross-section geometry and end support conditions on the post-buckling behavior and Direct Strength Method (DSM) design of cold-formed steel lipped channel and rack-section columns buckling and failing in distortional modes. The columns analyzed exhibited (i) four end support conditions, (ii) seven geometries (length and cross-section shape/dimensions – *4* lipped channels and *3* rack-sections) and (iii) several yield stresses. These characteristics were carefully selected (i) to ensure, as much as possible, "pure" distortional buckling and failure modes and (ii) to cover a wide (distortional) slenderness range. The ultimate strength data acquired during the performance of a parametric study involving *168* columns were then used to show that, regardless of the column geometry, the current DSM distortional design curve is only able to predict adequately (safely and accurately) the ultimate loads of fixed columns. For pinned-fixed, pinned and fixed-free columns, this design curve clearly overestimates the numerical ultimate loads in the high slenderness range ($\overline{\lambda}_D \geq 1.5$).

Therefore, adequate ultimate strength estimates for pinned-fixed, pinned and fixed-free columns can only be achieved by modifying the current DSM design curve. On the basis of the results obtained from the limited parametric study carried out in this work, modified distortional design curves were proposed for (i) pinned-fixed and pinned columns, and (ii) fixed-free columns, respectively. The ultimate strength estimates provided by these design curves correlated fairly well with the numerical ultimate loads obtained from the ANSYS non-linear shell finite element analyses.

Finally, one last word to mention that the authors plan to extend the scope of this investigation, by (i) analyzing lipped channel and rack-section columns that exhibit wider ranges of lengths and cross-section dimensions, and (ii) considering other commonly used cross-section shapes (*e.g.*, zed and hat-sections). The corresponding results and ensuing design proposals should be reported in the not too distant future.

References

ABNT (2010). *Brazilian Standard on Design of Cold-Formed Steel Structures* (ABNT NBR 14762:2010), Brazilian Association of Standards (ABNT), Rio de Janeiro, Brazil. (Portuguese)

AS/NZS (2005). *Cold-Formed Steel Structures*, Standards of Australia (SA) and Standards of New Zealand (SNZ), Sydney-Wellington.

Bebiano R, Pina P, Silvestre N, Camotim D (2008). *GBTUL 1.0β – Buckling and Vibration Analysis of Thin-Walled Members*, DECivil/IST, Technical University of Lisbon. (http://www.civil.ist.utl.pt/gbt)

Bebiano R, Silvestre N, Camotim D (2008). "GBTUL – A code for the buckling analysis of cold-formed steel members", *Proceedings of 19th International Specialty Conference on Recent Research and Developments in Cold-Formed Steel Design and Construction* (St. Louis, 14-15/10), R. LaBoube, W.W. Yu (eds.), 61-79.

Dinis PB, Camotim D (2006). "On the use of shell finite element analysis to assess the local buckling and post-buckling behaviour of cold-formed steel thin-walled members", *Abstracts of III European Conference on Computational Mechanics: Solids, Structures and Coupled Problems in Engineering* (III ECCM – Lisboa, 5-9/6), C.A.M. Soares *et al.* (eds.), Springer (Wien), 689. (full paper in CD-ROM Proceedings)

Dinis PB, Silvestre N, Camotim D (2009). "On the relevance of local/distortional interaction in the post-buckling behaviour and strength of cold-formed steel lipped channel columns", *Proceedings of Twelfth International Conference on Civil, Structural and Environmental Engineering Computing* (CC 2009 – Funchal, 1-4/9), B. Topping. L.C. Neves, R.C. Barros (eds.), Civil-Comp Press (Stirling), p. 22. (full paper in CD-ROM Proceedings)

Hancock GJ, Kwon YB, Bernard ES (1994). "Strength design curves for thin-walled sections undergoing distortional buckling", *Journal of Constructional Steel Research*, **31**(2-3), 169-186.

Kwon YB, Kim BS, Hancock GJ (2009). "Compression tests of high strength cold-formed steel channels with buckling interaction", *Journal of Constructional Steel Research*, **65**(2), 278–89.

Landesmann A, Camotim D (2010a). "Distortional failure and design of cold-formed steel lipped channel columns under fire conditions", *Proceedings of SSRC Annual Stability Conference* (Orlando, 12-15/5), 505-532.

Landesmann A, Camotim D (2010b). "Distortional failure and design of cold-formed steel rack-section columns under fire conditions", *Proceedings of 4th International Conference on Steel & Composite Structures* (ICSCS'2011 – Sydney, 21-23/7), B. Uy *et al.* (eds.), 287-289. (full paper in CD-ROM Proceedings)

Landesmann A, Camotim D (2011). "On the distortional buckling, post-buckling and strength of cold-formed steel lipped channel columns under fire conditions", *Journal of Structural Fire Engineering*, **2**(1), 1-19.

NAS (2007). *North American Specification for the Design of Cold-Formed Steel Structural Members* (AISI-S100-07), American Iron and Steel Institute (AISI), Washington DC.

Prola LC, Camotim D (2002a). "On the distortional post-buckling behavior of cold-formed lipped channel steel columns", *Proceedings of SSRC Annual Stability Conference* (Seattle, 24-27/4), 571-590.

Prola LC, Camotim D (2002b). "On the distortional post-buckling behaviour of rack-section cold-formed steel columns", *Proceedings of Sixth International Conference on Computational Structures Technology* (CST 2002 – Prague, 4-6/9), B. Topping, Z. Bittnar (eds.), Civil-Comp Press (Stirling), 233-234. (full paper in CD-ROM Proceedings - paper 98)

SAS (2004). *ANSYS Reference Manual*, Swanson Analysis Systems (SAS), version 8.1.

Schafer BW (2000). *Distortional Buckling of Cold-Formed Steel Columns*, American Iron and Steel Institute (AISI) Report, Washington DC.

Schafer BW (2003). "Advances in the direct strength design of thin-walled members", *Advances in Structures* (ASSCCA'03 – Sydney, 23-25/6), G.J. Hancock *et al.* (eds.), Balkema (Lisse), 333-339.

Schafer BW (2005). *Direct Strength Method Design Guide*, American Iron and Steel Institute (AISI) Report, Washington DC.

Schafer BW (2008). "Review: the Direct Strength Method of cold-formed steel member design", *Journal of Constructional Steel Research*, **64**(7-8), 766-788.

Schafer BW, Peköz T (1998). "Direct strength prediction of cold-formed steel members using numerical elastic buckling solutions", *Proceedings of 14th International Specialty Conference on Cold-formed Steel Structures* (St. Louis, 15-16/10), R. LaBoube, W.-W. Yu (eds.), 69-76.

Silvestre N, Camotim D, Dinis PB (2009a). "Direct strength prediction of lipped channel columns experiencing local-plate/distortional interaction", *Advanced Steel Construction – an International Journal*, **5**(1), 45-67.

Silvestre N, Camotim D, Young B (2009b). "Ultimate strength and design of lipped channel columns experiencing local/distortional mode interaction – part II: DSM design approach", *Proceedings of Sixth International Conference on Advances in Steel Structures* (ICASS'09 – Hong Kong, 16-18/12), S.L. Chan (ed.), Hong Kong Institute of Steel Construction, 470-479.

Young B, Camotim D, Silvestre N (2009). "Ultimate strength and design of lipped channel columns experiencing local/distortional mode interaction – part I: experimental investigation", *Proceedings of Sixth International Conference on Advances in Steel Structures* (ICASS'09 – Hong Kong, 16-18/12), S.L. Chan (ed.), Hong Kong Institute of Steel Construction, 460-469.

Annex

Tables A1 (F columns), A2 (P-F columns), A3 (P columns) and A4 (F-F columns) summarize the numerical (ANSYS shell finite element analysis) and DSM results obtained in the course of this research work. Each of them concerns seven column geometries and provides the corresponding (i) critical (distortional) buckling loads ($P_{cr.D}$), (ii) DSM ultimate strength estimates associated with global ($P_{n.e}$), interactive local/global ($P_{n.Le}$) and distortional ($P_{n.D}$), as well as the respective slenderness values ($\overline{\lambda}_e$, $\overline{\lambda}_{Le}$, $\overline{\lambda}_D$), (iii) numerically obtained failure mode natures, which may be either distortional (D), interactive local/global (L+G) or interactive local/distortional (L+D), (iv) squash loads (P_y), (v) absolute (P_u) and normalized (P_u/P_y) ultimate loads, (vi) normalized DSM distortional ultimate strength estimates ($P_{n.D}/P_y$) and (vii) DSM-to-numerical ultimate load ratios ($P_{n.D}/P_u$).

Finally, Table A5 concerns P-F, P and F-F columns and presents the (i) distortional slenderness values $\overline{\lambda}_D$, (ii) normalized numerical ultimate loads (P_u/P_y) and (iii) ratios between the ultimate strength estimates provided by the proposed modified DSM distortional design curves and the numerical ultimate loads ($P^*_{n.D}/P_u$ and $P^{**}_{n.D}/P_u$).

Table A1: Numerical and DSM results concerning the behavior and strength of the F columns.

Column	$P_{cr.D}$ (kN)	$\bar{\lambda}_e$	$P_{n.e}$ (kN)	$\bar{\lambda}_D$	$P_{n.D}$ (kN)	$\bar{\lambda}_{Le}$	$P_{n.Le}$ (kN)	$P_{u.DSM}$ (kN)	*Failure*	P_y (kN)	P_u (kN)	$\frac{P_u}{P_y}$	$\frac{P_{n.D}}{P_y}$	$\frac{P_{n.D}}{P_u}$
C75	211.8	0.21	120.2	0.76	111.1	0.64	120.2	111.1	D	122.5	115.5	0.94	0.91	0.96
		0.31	258.6	1.13	182.8	0.94	228.4	182.8	D	269.5	188.6	0.70	0.68	0.97
		0.35	325.4	1.27	208.8	1.06	266.4	208.8	D	343.0	218.6	0.64	0.61	0.95
		0.46	537.2	1.67	275.5	1.36	370.9	275.5	L+D	588.0	286.0	0.49	0.47	0.96
		0.54	695.0	1.92	316.7	1.55	438.5	316.7	L+D	784.0	323.9	0.41	0.40	0.98
		0.60	843.0	2.15	351.9	1.70	496.7	351.9	L+D	980.0	355.7	0.36	0.36	0.99
C100	473.2	0.33	157.4	0.59	164.4	0.49	157.4	157.4*	D	165.0	163.3	0.99	1.00	1.01
		0.50	327.4	0.88	300.9	0.71	327.4	300.9	D	363.0	339.9	0.94	0.83	0.89
		0.56	405.1	0.99	349.8	0.79	400.3	349.8	D	462.0	395.2	0.86	0.76	0.89
		0.73	632.2	1.29	474.7	0.99	541.6	474.7	L+D	792.0	521.8	0.66	0.60	0.91
		0.85	781.9	1.49	551.6	1.10	624.3	551.6	L+D	1056.0	594.9	0.56	0.52	0.93
		0.95	906.6	1.67	616.9	1.18	688.6	616.9	L+D	1320.0	649.7	0.49	0.47	0.95
C120	244.2	0.28	175.3	0.86	152.0	0.73	175.3	152.0	D	181.3	167.4	0.92	0.84	0.91
		0.42	370.5	1.28	241.8	1.06	302.4	241.8	L+D	398.8	269.3	0.68	0.61	0.90
		0.47	462.1	1.44	274.5	1.19	350.2	274.5	L+D	507.5	297.0	0.59	0.54	0.92
		0.62	741.0	1.89	358.6	1.50	476.9	358.6	L+D	870.0	350.5	0.40	0.41	1.02
		0.71	936.6	2.18	410.8	1.69	554.9	410.8	L+D	1160.0	379.4	0.33	0.35	1.08
		0.80	1109.7	2.44	455.2	1.84	618.7	455.2	L+D	1450.0	451.1	0.31	0.31	1.01
C130	136.0	0.38	167.1	1.14	119.0	1.01	141.2	119.0	D	177.5	126.5	0.71	0.67	0.94
		0.56	341.7	1.69	179.8	1.44	226.4	179.8	L+D	390.5	176.1	0.45	0.46	1.02
		0.64	419.4	1.91	202.1	1.60	258.5	202.1	L+D	497.0	185.3	0.37	0.41	1.09
		0.83	636.8	2.50	259.7	1.97	338.0	259.7	L+D	852.0	241.1	0.28	0.30	1.08
		0.96	770.6	2.89	295.6	2.17	381.6	295.6	L+D	1136.0	275.2	0.24	0.26	1.07
		1.08	874.2	3.23	326.3	2.31	413.4	326.3	L+D	1420.0	283.9	0.20	0.23	1.15
R75	294.9	0.22	125.0	0.66	123.7	0.37	125.0	123.7	D	127.5	125.8	0.99	0.97	0.98
		0.32	268.8	0.98	214.6	0.54	268.8	214.6	D	280.5	256.0	0.91	0.77	0.84
		0.36	338.1	1.10	247.4	0.60	338.1	247.4	D	357.0	281.0	0.79	0.69	0.88
		0.47	557.6	1.44	331.2	0.78	557.6	331.2	L+D	612.0	330.2	0.54	0.54	1.00
		0.54	720.7	1.66	382.9	0.88	664.8	382.9	L+D	816.0	359.6	0.44	0.47	1.06
		0.61	873.3	1.86	426.9	0.97	757.0	426.9	L+D	1020.0	377.5	0.37	0.42	1.13
R100	702.0	0.32	272.9	0.64	279.3	0.54	272.9	272.9*	D	285.0	281.9	0.99	0.98	0.99
		0.48	569.9	0.95	491.5	0.78	566.2	491.5	D	627.0	582.6	0.93	0.78	0.84
		0.54	706.7	1.07	567.9	0.87	656.0	567.9	D	798.0	662.2	0.83	0.71	0.86
		0.71	1110.8	1.40	763.1	1.09	889.1	763.1	L+D	1368.0	859.1	0.63	0.56	0.89
		0.81	1381.8	1.61	883.5	1.22	1027.3	883.5	L+D	1824.0	883.6	0.48	0.48	1.00
		0.91	1611.4	1.80	985.9	1.32	1136.4	985.9	L+D	2280.0	912.7	0.40	0.43	1.08
R135	256.2	0.55	222.9	0.99	190.5	0.81	216.4	190.5	D	252.5	224.6	0.89	0.75	0.85
		0.81	422.1	1.47	294.3	1.12	332.9	294.3	L+D	555.5	303.7	0.55	0.53	0.97
		0.91	498.5	1.66	332.2	1.22	371.6	332.2	L+D	707.0	334.3	0.47	0.47	0.99
		1.20	665.7	2.17	430.1	1.41	449.2	430.1	L+D	1212.0	392.5	0.32	0.35	1.10
		1.38	727.0	2.51	490.9	1.47	475.6	475.6*	L+D	1616.0	400.3	0.25	0.30	1.23
		1.54	742.6	2.81	542.8	1.48	482.2	482.2*	L+D	2020.0	407.1	0.20	0.27	1.33

Table A2: Numerical and DSM results concerning the behavior and strength of the P-F columns.

Column	$P_{cr.D}$ (kN)	$\bar{\lambda}_e$	$P_{n.e}$ (kN)	$\bar{\lambda}_D$	$P_{n.D}$ (kN)	$\bar{\lambda}_{Le}$	$P_{n.Le}$ (kN)	$P_{u.DSM}$ (kN)	*Failure*	P_y (kN)	P_u (kN)	$\frac{P_u}{P_y}$	$\frac{P_{n.D}}{P_y}$	$\frac{P_{n.D}}{P_u}$
C75	146.51	0.36	116.0	0.91	98.4	0.64	116.0	98.4	D	122.5	101.7	0.83	0.80	0.97
		0.54	238.9	1.36	154.5	0.92	215.2	154.5	D	269.5	136.1	0.51	0.57	1.14
		0.60	294.3	1.53	175.0	1.02	247.5	175.0	D	343.0	139.9	0.41	0.51	1.25
		0.79	452.2	2.00	227.7	1.26	329.1	227.7	D	588.0	149.2	0.25	0.39	1.53
		0.91	552.4	2.31	260.4	1.39	375.2	260.4	D	784.0	158.2	0.20	0.33	1.65
		1.02	632.7	2.59	288.3	1.49	409.8	288.3	D	980.0	168.4	0.17	0.29	1.71
C100	493.94	0.25	160.8	0.58	164.8	0.50	160.8	160.8*	D	165.0	162.7	0.99	1.00	1.01
		0.37	342.8	0.86	305.4	0.73	342.8	305.4	D	363.0	310.3	0.85	0.84	0.98
		0.42	429.5	0.97	355.8	0.82	415.0	355.8	D	462.0	358.1	0.78	0.77	0.99
		0.55	698.9	1.27	484.3	1.05	576.8	484.3	D	792.0	440.5	0.56	0.61	1.10
		0.63	893.8	1.46	563.3	1.18	679.1	563.3	D	1056.0	471.9	0.45	0.53	1.19
		0.71	1071.6	1.63	630.4	1.29	765.2	630.4	D	1320.0	506.9	0.38	0.48	1.24
C120	217.60	0.40	169.4	0.91	145.8	0.72	169.4	145.8	D	181.3	148.9	0.82	0.80	0.98
		0.60	343.4	1.35	229.1	1.03	286.7	229.1	D	398.8	199.3	0.50	0.57	1.15
		0.67	419.6	1.53	259.4	1.14	327.6	259.4	D	507.5	207.0	0.41	0.51	1.25
		0.88	628.0	2.00	337.6	1.39	427.0	337.6	D	870.0	228.9	0.26	0.39	1.47
		1.02	751.2	2.31	386.1	1.52	479.7	386.1	L+D	1160.0	252.8	0.22	0.33	1.53
		1.14	842.3	2.58	427.4	1.61	516.5	427.4	L+D	1450.0	270.2	0.19	0.29	1.58
C130	117.16	0.48	161.0	1.23	111.4	1.00	137.0	111.4	D	177.5	98.8	0.56	0.63	1.13
		0.72	315.0	1.83	166.6	1.40	213.4	166.6	D	390.5	113.0	0.29	0.43	1.47
		0.81	378.0	2.06	186.9	1.53	240.3	186.9	D	497.0	117.2	0.24	0.38	1.59
		1.06	533.0	2.70	239.4	1.82	299.8	239.4	L+D	852.0	133.8	0.16	0.28	1.79
		1.22	607.8	3.11	272.1	1.94	326.1	272.1	L+D	1136.0	145.2	0.13	0.24	1.87
		1.37	649.8	3.48	300.0	2.01	340.3	300.0	L+D	1420.0	155.0	0.11	0.21	1.94
R75	240.58	0.33	121.9	0.73	118.3	0.58	121.9	118.3	D	127.5	125.0	0.98	0.93	0.95
		0.49	254.2	1.08	197.5	0.83	242.8	197.5	D	280.5	225.9	0.81	0.70	0.87
		0.55	314.9	1.22	226.1	0.93	280.9	226.1	D	357.0	239.4	0.67	0.63	0.94
		0.72	493.7	1.59	299.6	1.16	379.3	299.6	D	612.0	274.1	0.45	0.49	1.09
		0.83	612.7	1.84	345.0	1.30	437.3	345.0	L+D	816.0	293.9	0.36	0.42	1.17
		0.93	712.9	2.06	383.7	1.40	482.8	383.7	L+D	1020.0	305.5	0.30	0.38	1.26
R100	540.09	0.39	267.6	0.73	264.8	0.54	267.6	264.8	D	285.0	280.9	0.99	0.93	0.94
		0.58	545.7	1.08	442.3	0.78	545.2	442.3	D	627.0	519.1	0.83	0.71	0.85
		0.65	668.7	1.22	506.5	0.86	626.8	506.5	D	798.0	549.6	0.69	0.63	0.92
		0.85	1010.3	1.59	671.2	1.06	827.8	671.2	D	1368.0	619.8	0.45	0.49	1.08
		0.98	1217.6	1.84	772.9	1.16	937.0	772.9	D	1824.0	639.1	0.35	0.42	1.21
		1.10	1375.7	2.05	859.6	1.23	1015.6	859.6	D	2280.0	641.9	0.28	0.38	1.34
R135	235.10	0.57	220.6	1.04	184.0	0.82	213.7	184.0	D	252.5	207.9	0.82	0.73	0.88
		0.84	412.8	1.54	282.1	1.12	325.9	282.1	D	555.5	242.5	0.44	0.51	1.16
		0.95	484.5	1.73	318.0	1.21	362.3	318.0	L+D	707.0	254.7	0.36	0.45	1.25
		1.24	634.1	2.27	410.7	1.38	432.2	410.7	L+D	1212.0	284.0	0.23	0.34	1.45
		1.44	681.3	2.62	468.3	1.44	452.9	452.9*	L+D	1616.0	292.7	0.18	0.29	1.60
		1.61	686.7	2.93	517.5	1.44	455.3	455.3*	L+D	2020.0	293.9	0.15	0.26	1.76

Table A3: Numerical and DSM results concerning the behavior and strength of the P columns.

Column	$P_{cr.D}$ (kN)	$\bar{\lambda}_e$	$P_{n.e}$ (kN)	$\bar{\lambda}_D$	$P_{n.D}$ (kN)	$\bar{\lambda}_{Le}$	$P_{n.Le}$ (kN)	$P_{u.DSM}$ (kN)	*Failure*	P_y (kN)	P_u (kN)	$\frac{P_u}{P_y}$	$\frac{P_{n.D}}{P_y}$	$\frac{P_{n.D}}{P_u}$
C75	128.22	0.37	115.8	0.98	93.6	0.64	115.8	93.6	D	122.5	109.7	0.90	0.76	0.85
		0.54	238.1	1.45	145.0	0.92	214.2	145.0	D	269.5	137.3	0.51	0.54	1.06
		0.61	293.0	1.64	163.7	1.02	246.2	163.7	D	343.0	140.3	0.41	0.48	1.17
		0.80	448.9	2.14	212.2	1.26	326.7	212.2	D	588.0	145.7	0.25	0.36	1.46
		0.93	547.0	2.47	242.2	1.39	371.8	242.2	D	784.0	157.3	0.20	0.31	1.54
		1.04	624.8	2.76	267.9	1.49	405.5	267.9	D	980.0	167.5	0.17	0.27	1.60
C100	446.73	0.20	162.3	0.61	163.6	0.51	162.3	162.3*	D	165.0	163.2	0.99	0.99	1.00
		0.29	350.0	0.90	294.7	0.74	350.0	294.7	D	363.0	309.8	0.85	0.81	0.95
		0.33	441.1	1.02	341.8	0.83	421.4	341.8	D	462.0	343.4	0.74	0.74	1.00
		0.44	731.5	1.33	462.1	1.07	592.8	462.1	D	792.0	406.1	0.51	0.58	1.14
		0.50	949.9	1.54	536.2	1.22	704.7	536.2	D	1056.0	446.8	0.42	0.51	1.20
		0.56	1156.3	1.72	599.1	1.35	801.7	599.1	D	1320.0	477.6	0.36	0.45	1.25
C120	201.23	0.24	176.8	0.95	141.6	0.74	176.8	141.6	D	181.3	144.8	0.80	0.78	0.98
		0.36	377.4	1.41	220.7	1.08	304.3	220.7	D	398.8	187.4	0.47	0.55	1.18
		0.41	473.2	1.59	249.5	1.21	353.4	249.5	D	507.5	193.1	0.38	0.49	1.29
		0.54	771.7	2.08	323.9	1.55	486.3	323.9	D	870.0	225.4	0.26	0.37	1.44
		0.62	988.6	2.40	370.1	1.75	570.6	370.1	D	1160.0	246.7	0.21	0.32	1.50
		0.69	1187.3	2.68	409.5	1.92	641.6	409.5	D	1450.0	262.8	0.18	0.28	1.56
C130	110.01	0.35	168.8	1.27	108.2	1.03	140.6	108.2	D	177.5	98.7	0.56	0.61	1.10
		0.51	349.7	1.88	161.3	1.48	227.2	161.3	D	390.5	105.1	0.27	0.41	1.53
		0.58	431.9	2.13	180.8	1.65	260.4	180.8	D	497.0	110.5	0.22	0.36	1.64
		0.76	669.7	2.78	231.2	2.05	344.9	231.2	D	852.0	124.4	0.15	0.27	1.86
		0.88	824.0	3.21	262.7	2.28	393.5	262.7	D	1136.0	137.0	0.12	0.23	1.92
		0.98	950.6	3.59	289.5	2.45	430.7	289.5	D	1420.0	143.3	0.10	0.20	2.02
R75	193.49	0.39	119.7	0.81	111.2	0.57	119.7	111.2	D	127.5	121.6	0.95	0.87	0.91
		0.58	243.9	1.20	179.6	0.82	235.8	179.6	D	280.5	187.5	0.67	0.64	0.96
		0.65	298.9	1.36	204.4	0.91	270.8	204.4	D	357.0	194.9	0.55	0.57	1.05
		0.85	451.3	1.78	268.3	1.11	356.9	268.3	D	612.0	209.3	0.34	0.44	1.28
		0.99	543.6	2.05	307.8	1.22	403.6	307.8	D	816.0	215.8	0.26	0.38	1.43
		1.10	613.9	2.30	341.5	1.30	437.2	341.5	D	1020.0	218.8	0.21	0.33	1.56
R100	435.56	0.47	260.1	0.81	249.1	0.54	260.1	249.1	D	285.0	275.1	0.97	0.87	0.91
		0.69	512.8	1.20	402.7	0.76	512.8	402.7	D	627.0	432.0	0.69	0.64	0.93
		0.78	617.9	1.35	458.4	0.83	592.2	458.4	D	798.0	448.6	0.56	0.57	1.02
		1.02	882.3	1.77	601.8	0.99	753.9	601.8	D	1368.0	472.7	0.35	0.44	1.27
		1.18	1016.5	2.05	690.6	1.06	828.8	690.6	D	1824.0	474.9	0.26	0.38	1.45
		1.32	1097.8	2.29	766.3	1.11	872.3	766.3	D	2280.0	474.9	0.21	0.34	1.61
R135	211.34	0.42	234.1	1.09	175.9	0.88	216.1	175.9	D	252.5	199.9	0.79	0.70	0.88
		0.63	470.4	1.62	267.5	1.25	344.4	267.5	D	555.5	214.9	0.39	0.48	1.24
		0.71	572.2	1.83	301.1	1.38	391.5	301.1	D	707.0	222.4	0.31	0.43	1.35
		0.93	843.3	2.39	387.7	1.67	503.5	387.7	D	1212.0	248.1	0.20	0.32	1.56
		1.07	996.4	2.77	441.7	1.82	560.4	441.7	D	1616.0	257.4	0.16	0.27	1.72
		1.20	1103.7	3.09	487.7	1.91	598.3	487.7	D	2020.0	258.2	0.13	0.24	1.89

Table A4: Numerical and DSM results concerning the behavior and strength of the F-F columns.

Column	$P_{cr.D}$ (kN)	$\bar{\lambda}_e$	$P_{n.e}$ (kN)	$\bar{\lambda}_D$	$P_{n.D}$ (kN)	$\bar{\lambda}_{Le}$	$P_{n.Le}$ (kN)	$P_{u.DSM}$ (kN)	*Failure*	P_y (kN)	P_u (kN)	$\frac{P_u}{P_y}$	$\frac{P_{n.D}}{P_y}$	$\frac{P_{n.D}}{P_u}$
C75	80.84	0.38	115.5	1.21	78.0	0.74	115.5	78.0	D	122.5	78.1	0.64	0.64	1.00
		0.56	236.6	1.80	116.9	1.06	193.8	116.9	D	269.5	86.0	0.32	0.43	1.36
		0.63	290.6	2.03	131.2	1.17	222.1	131.2	D	343.0	88.7	0.26	0.38	1.48
		0.82	442.6	2.65	168.2	1.45	292.6	168.2	D	588.0	96.7	0.16	0.29	1.74
		0.95	536.9	3.06	191.2	1.59	331.6	191.2	D	784.0	102.4	0.13	0.24	1.87
		1.06	610.5	3.43	210.9	1.70	360.3	210.9	D	980.0	107.5	0.11	0.22	1.96
C100	257.47	0.28	159.5	0.80	145.1	0.60	159.5	145.1	D	165.0	144.6	0.88	0.88	1.00
		0.42	336.9	1.19	235.3	0.88	312.2	235.3	D	363.0	215.0	0.59	0.65	1.09
		0.48	420.1	1.34	268.0	0.98	362.4	268.0	D	462.0	227.1	0.49	0.58	1.18
		0.62	672.9	1.75	352.2	1.24	495.7	352.2	D	792.0	250.4	0.32	0.44	1.41
		0.72	849.7	2.03	404.3	1.39	577.6	404.3	D	1056.0	267.4	0.25	0.38	1.51
		0.81	1006.0	2.26	448.6	1.51	644.6	448.6	D	1320.0	284.6	0.22	0.34	1.58
C120	125.38	0.32	173.6	1.20	116.2	0.87	161.1	116.2	D	181.3	111.0	0.61	0.64	1.05
		0.48	362.7	1.78	174.3	1.26	263.4	174.3	D	398.8	126.3	0.32	0.44	1.38
		0.54	449.8	2.01	195.6	1.41	303.3	195.6	D	507.5	133.1	0.26	0.39	1.47
		0.70	707.4	2.63	250.8	1.76	406.5	250.8	D	870.0	155.4	0.18	0.29	1.61
		0.81	880.4	3.04	285.2	1.97	467.6	285.2	D	1160.0	169.1	0.15	0.25	1.69
		0.91	1027.2	3.40	314.6	2.13	515.8	314.6	D	1450.0	180.5	0.12	0.22	1.74
C130	62.34	0.46	162.4	1.69	82.1	1.18	123.8	82.1	D	177.5	64.3	0.36	0.46	1.28
		0.68	321.1	2.50	119.1	1.65	193.1	119.1	D	390.5	74.9	0.19	0.30	1.59
		0.77	387.5	2.82	132.7	1.82	217.9	132.7	D	497.0	79.8	0.16	0.27	1.66
		1.01	556.0	3.70	168.2	2.18	274.4	168.2	D	852.0	91.9	0.11	0.20	1.83
		1.17	643.0	4.27	190.4	2.34	300.9	190.4	D	1136.0	98.1	0.09	0.17	1.94
		1.30	697.2	4.77	209.3	2.44	316.7	209.3	D	1420.0	102.9	0.07	0.15	2.03
R75	130.53	0.47	116.4	0.99	96.2	0.67	116.4	96.2	D	127.5	98.0	0.77	0.75	0.98
		0.69	229.6	1.47	148.6	0.95	202.3	148.6	D	280.5	118.1	0.42	0.53	1.26
		0.78	276.6	1.66	167.8	1.04	229.3	167.8	D	357.0	120.2	0.34	0.47	1.40
		1.02	395.2	2.17	217.2	1.24	290.4	217.2	D	612.0	121.6	0.20	0.35	1.79
		1.18	455.5	2.51	247.9	1.33	318.8	247.9	D	816.0	121.6	0.15	0.30	2.04
		1.32	492.1	2.81	274.1	1.39	335.3	274.1	D	1020.0	121.6	0.12	0.27	2.25
R100	291.57	0.52	254.0	0.99	215.7	0.63	254.0	215.7	D	285.0	234.7	0.82	0.76	0.92
		0.78	486.5	1.47	333.5	0.87	453.0	333.5	D	627.0	264.3	0.42	0.53	1.26
		0.88	577.8	1.65	376.6	0.95	509.0	376.6	D	798.0	264.9	0.33	0.47	1.42
		1.15	786.4	2.17	487.6	1.10	625.7	487.6	D	1368.0	264.9	0.19	0.36	1.84
		1.33	871.8	2.50	556.6	1.16	669.9	556.6	D	1824.0	262.8	0.14	0.31	2.12
		1.48	906.1	2.80	615.5	1.19	687.2	615.5	D	2280.0	264.9	0.12	0.27	2.32
R135	114.43	0.54	223.3	1.49	132.6	1.03	186.6	132.6	D	252.5	111.5	0.44	0.53	1.19
		0.80	424.0	2.20	194.4	1.41	284.8	194.4	D	555.5	111.5	0.20	0.35	1.74
		0.91	501.3	2.49	217.2	1.54	317.6	217.2	D	707.0	113.8	0.16	0.31	1.91
		1.19	672.2	3.25	276.3	1.78	383.7	276.3	D	1212.0	121.1	0.10	0.23	2.28
		1.37	736.4	3.76	313.1	1.86	406.8	313.1	D	1616.0	128.8	0.08	0.19	2.43
		1.53	754.7	4.20	344.7	1.89	413.2	344.7	D	2020.0	136.4	0.07	0.17	2.53

Table A5: Numerical ultimate loads and modified DSM predictions concerning the P-F, P and F-F columns

Column	*Pinned-Fixed*				*Pinned*				*Fixed-Free*			
	$\bar{\lambda}_D$	$\frac{P_u}{P_y}$	$\frac{P^*_{n.D}}{P_u}$	$\frac{P^{**}_{n.D}}{P_u}$	$\bar{\lambda}_D$	$\frac{P_u}{P_y}$	$\frac{P^*_{n.D}}{P_u}$	$\frac{P^{**}_{n.D}}{P_u}$	$\bar{\lambda}_D$	$\frac{P_u}{P_y}$	$\frac{P^*_{n.D}}{P_u}$	$\frac{P^{**}_{n.D}}{P_u}$
C75	0.91	0.83	0.97	0.97	0.98	0.90	0.85	0.85	1.23	0.64	0.97	0.94
	1.36	0.51	0.97	0.97	1.45	0.51	0.84	0.86	1.83	0.32	0.87	0.95
	1.53	0.41	0.93	0.98	1.64	0.41	0.81	0.87	2.06	0.26	0.85	0.96
	2.00	0.25	0.88	1.00	2.14	0.25	0.80	0.92	2.70	0.16	0.81	0.98
	2.31	0.20	0.85	1.00	2.47	0.20	0.75	0.90	3.11	0.13	0.79	0.98
	2.59	0.17	0.81	0.98	2.76	0.17	0.72	0.88	3.48	0.11	0.77	0.98
C100	0.58	0.99	1.01	1.01	0.61	0.99	1.00	1.00	0.80	0.88	1.00	1.00
	0.86	0.85	0.98	0.98	0.90	0.85	0.95	0.95	1.19	0.59	1.09	1.05
	0.97	0.78	0.99	0.99	1.02	0.74	1.00	1.00	1.34	0.49	1.02	1.02
	1.27	0.56	1.02	1.00	1.33	0.51	0.99	0.99	1.75	0.32	0.92	1.00
	1.46	0.45	0.94	0.97	1.54	0.42	0.89	0.94	2.03	0.25	0.87	0.99
	1.63	0.38	0.87	0.93	1.72	0.36	0.83	0.91	2.26	0.22	0.83	0.96
C120	0.91	0.82	0.98	0.98	0.95	0.80	0.98	0.98	1.20	0.61	1.03	0.99
	1.35	0.50	0.98	0.99	1.41	0.47	0.96	0.98	1.78	0.32	0.89	0.97
	1.53	0.41	0.94	0.98	1.59	0.38	0.93	0.98	2.01	0.26	0.85	0.96
	2.00	0.26	0.86	0.97	2.08	0.26	0.81	0.92	2.63	0.18	0.75	0.91
	2.31	0.22	0.79	0.92	2.40	0.21	0.75	0.89	3.04	0.15	0.71	0.89
	2.58	0.19	0.75	0.90	2.68	0.18	0.72	0.87	3.40	0.12	0.69	0.87
C130	1.23	0.56	1.08	1.05	1.27	0.56	1.01	0.99	1.69	0.36	0.86	0.93
	1.83	0.29	0.93	1.02	1.88	0.27	0.94	1.05	2.50	0.19	0.77	0.92
	2.06	0.24	0.90	1.03	2.13	0.22	0.90	1.04	2.82	0.16	0.74	0.91
	2.70	0.16	0.82	1.00	2.78	0.15	0.84	1.02	3.70	0.11	0.69	0.88
	3.11	0.13	0.78	0.98	3.21	0.12	0.78	0.99	4.27	0.09	0.67	0.88
	3.48	0.11	0.75	0.96	3.59	0.10	0.77	0.99	4.77	0.07	0.66	0.89
R75	0.73	0.98	0.95	0.95	0.81	0.95	0.91	0.91	0.99	0.77	0.98	0.98
	1.08	0.81	0.87	0.87	1.20	0.67	0.94	0.91	1.47	0.42	0.98	1.01
	1.22	0.67	0.92	0.89	1.36	0.55	0.89	0.90	1.65	0.34	0.96	1.03
	1.59	0.45	0.78	0.83	1.78	0.34	0.83	0.91	2.17	0.20	0.97	1.12
	1.84	0.36	0.73	0.81	2.05	0.26	0.81	0.92	2.50	0.15	0.99	1.18
	2.06	0.30	0.71	0.81	2.30	0.21	0.81	0.95	2.80	0.12	1.01	1.23
R100	0.73	0.99	0.94	0.94	0.81	0.97	0.91	0.91	0.99	0.82	0.92	0.92
	1.08	0.83	0.85	0.85	1.20	0.69	0.92	0.89	1.47	0.42	0.99	1.02
	1.22	0.69	0.90	0.87	1.35	0.56	0.87	0.88	1.65	0.33	0.98	1.05
	1.59	0.45	0.78	0.82	1.77	0.35	0.82	0.90	2.17	0.19	1.00	1.15
	1.84	0.35	0.76	0.84	2.05	0.26	0.83	0.94	2.50	0.14	1.03	1.23
	2.05	0.28	0.76	0.87	2.29	0.21	0.84	0.98	2.80	0.12	1.04	1.28
R135	1.09	0.82	0.88	0.88	1.09	0.79	0.88	0.88	1.49	0.44	0.92	0.95
	1.62	0.44	0.86	0.91	1.62	0.39	0.88	0.94	2.20	0.20	0.93	1.08
	1.83	0.36	0.82	0.90	1.83	0.31	0.85	0.94	2.49	0.16	0.93	1.11
	2.39	0.23	0.76	0.88	2.39	0.20	0.78	0.93	3.25	0.10	0.92	1.17
	2.76	0.18	0.75	0.91	2.77	0.16	0.78	0.95	3.76	0.08	0.90	1.17
	3.09	0.15	0.76	0.94	3.09	0.13	0.79	0.99	4.20	0.07	0.88	1.16